Diurnal rhythmicity of fecal microbiota and metabolite profiles in the first year of life: a randomized controlled interventional trial with infant formula

Nina Heppner[1,2], Sandra Reitmeier[1,2], Marjolein Heddes[1,2], Michael Vig Merino[1,2], Leon Schwartz[3], Alexander Dietrich[3], Markus List[3], Michael Gigl[4], Chen Meng[4], Hélène Omer[1,2], Karin Kleigrewe[4], Melanie Schirmer[2], Daan R van der Veen[5], Silke Kiessling[1,2,5*], Dirk Haller [1,2*]

[1] Chair of Nutrition and Immunology, Technical University of Munich, Gregor-Mendel-Str. 2, 85354 Freising, Germany

[2] ZIEL - Institute for Food & Health, Technical University of Munich, 85354 Freising, Germany

[3] Data Science in Systems Biology, School of Life Sciences, Technical University of Munich, 85354 Freising, Germany

[4] Bavarian Center for Biomolecular Mass Spectrometry, Technical University of Munich, Gregor-Mendel-Str. 4, 85354 Freising, Germany

[5] Faculty of Health and Biomedical Science, University of Surrey, 388 Stag Hill Campus, 17 GU27XH, Guildford, United Kingdom

* Authors contributed equally

Correspondence:
Prof. Dr. Dirk Haller
Technical University of Munich
Chair of Nutrition and Immunology
Gregor-Mendel-Str. 2
85354 Freising, Germany
Email: dirk.haller@tum.de
Phone: + 49 8161-71 2026

Keywords

Circadian rhythmicity, infant microbiome, untargeted metabolomics, Bifidobacteria, Galacto-oligosaccharides, intervention trial, infant formula, gut chemostat

Summary

Microbiota assembly in the infant gut is influenced by time and duration of dietary exposure to breast-milk, infant formula and solid foods. In this randomized controlled intervention study, longitudinal sampling of infant stool (n=998) showed similar development of fecal bacterial communities (16S rRNA/shallow metagenomics sequencing) between formula- and breast-fed infants during the first year of life (N=210). Infant formula supplemented with galacto-oligosaccharides (GOS) was most efficient to sustain high levels of bifidobacteria compared to formula containing *B. longum* and *B. breve* or placebo. In addition to primary endpoints, metabolite and bacterial profiling revealed 24-hour oscillations and data integration identified circadian networks. Rhythmicity in bacterial diversity, specific taxa and functional pathways increased with age and was strongest following breast-feeding and GOS-supplementation. Circadian rhythms in dominant taxa were discovered *ex-vivo* in a chemostat model. Hence, microbiota rhythmicity develops early in life, likely via bacterial intrinsic clock mechanism and is affected by diet.

Main

Characteristic of the developing infant gut microbiota is the high degree of individual variation during the first years of life[1]. The deterministic or stochastic succession of microbial communities in the healthy infant gut is largely linked to environmental and dietary exposures[2-4]. Colonization of the sterile infant gut starts at birth and depends on fetal exposure to microbial metabolites from the mother (immune imprinting)[5], birth mode, and the presence of microbial pioneers from the fecal, vaginal or skin environment[3]. Timing and duration of breast- and formula feeding are subsequent drivers of early life microbial succession[6,7]. Breast-fed infants are typically characterized by low bacterial diversity and dominance of bifidobacteria[8-10]. Human breastmilk oligosaccharides (HMOs) selectively shape the early life colonization[11-13] and the supplementation of infant formula with complex oligosaccharides such as galacto-oligosaccharides (GOS) partially mimics the effect of breastmilk[14,15]. Considering the well-documented effects of the early life microbiota on health outcomes later in life[8,16,17], the attempts to optimize infant formula are numerous[18-21] but often lack well-controlled intervention strategies to directly compare supplements in infant formula.

Circadian clocks (lat. *circa* = approximately, *dies* = day) have developed in almost all organisms to anticipate recurring environmental changes. In mammals, a central clock in the brain orchestrates subordinated peripheral clocks of various tissues and single cells[22]. Thereby the circadian system drives 24-hour oscillations to control body and organ functions, however, the contribution of circadian rhythms in the developing gut including the process of microbial colonization is completely unknown[23]. So far, circadian clock mechanisms were believed to be restricted to photosynthetic bacteria, such as cyanobacteria, but, in single bacterial cultures circadian oscillations were found in gene expression of non-photosynthetic *Bacillus subtilis*[24] and swarming behavior of the gut bacterium *Klebsiella aerogenes*[25], suggesting the presence of endogenous circadian clocks in specific gut bacteria. In recent years, time-of-day dependent fluctuations in the abundance of certain gut bacterial species were shown at the individual and population level[26,27]. Growing evidence provides a link between loss of rhythmicity and disease pathology[27]. Animal studies determined the origin of these bacterial oscillations to reside in the circadian system[28-30], particularly the intestinal circadian clock[31]. The mammalian circadian

system develops *in utero,* which continues during aging and plays an important role during development[32]. Gut microbiota rhythms can influence clock gene expression in the host [33,34] and disturbance of the circadian crosstalk between bacteria and the host was shown to affect gastrointestinal health and metabolism[30,31,34]. Whether bacteria endogenous clock mechanisms can drive rhythmicity of complex microbiota and thereby impact host physiology remains unknown.

Here we established a randomized, controlled intervention trial including 210 infants to address the role of cow's-milk based infant formula supplemented with bifidobacteria and GOS on early life development of the gut microbiota. Longitudinal sampling of infant stool (n=998) allowed us to temporally resolve microbiota and metabolite profiles in response to the supplemented infant formula. Exclusively breast-fed infants served as a reference group to evaluate the impact of infant formula feeding. In addition to the analysis of primary endpoints, we identified diurnal oscillations of the microbiome in relation to dietary exposure and confirmed the circadian rhythmicity of dominant taxa *ex-vivo* in a gut chemostat model.

Results

Eligibility assessment of 265 pregnant women led to the inclusion of 223 infants in the intervention study. Of those infants, 210 actively participated and were randomly assigned to one of the four different formula groups (**Fig. 1**). 63 infants were breast-fed for the duration of the intervention (1 year). 35 infants were randomized to receive the placebo containing no additional supplements (Formula A), 39 infants were randomized to Formula B containing *B. longum* and *B. breve*, 36 infants received formula containing prebiotics (GOS) (Formula C) and 37 infants consumed formula containing both bifidobacteria and GOS (Formula D) (**Fig. 1**). Fecal samples were collected at five time points during the first year of life (**Fig. 2A**). 87% of participants contributed to all sampling time points. An additional, voluntary follow-up sample was provided by 93 participants at the 24-month time point (29 breast-fed, 15 formula A-fed, 16 formula B-fed, 17 formula C-fed, 16 formula D-fed infants). The characteristics of participants in the five study arms were comparable (**Table 1**) and the weight gain of infants was similar across groups (**Suppl. Fig. 1A**). Daily formula amounts consumed were similar across interventional groups (**Suppl. Fig. 1B-C**). Differences in breastmilk metabolites over 103 samples could not classify the corresponding infant fecal metabolite profiles (**Suppl. Fig. 1D-E**). Rates for study discontinuation were low (**Table 1**) with suspected cow's milk protein allergy (6 out of 9 cases) being the main reason for study withdrawal.

Temporal development of infant microbiota

Longitudinal infant and parental fecal sampling (n_i=998; n_p=152) demonstrated that the temporal assembly of infant microbiota developed towards the parental microbial composition (**Fig. 2B-D, Suppl. Fig. 2A**). Supervised beta-diversity analysis illustrated significant shifts of microbiota profiles at month 3-24, yet showing clearly distinct patterns compared to parental samples, whereas the early sampling time points (0.5, 1 and 3 months) were characterized by indistinguishable clusters of microbiota profiles (**Fig. 2B**). Unsupervised analysis based on generalized UniFrac distances identified remarkable heterogeneity in microbiota profiles largely independent of the feeding type or birth groups (C-section vs vaginal birth) (**Fig. 2C**). Parental samples appeared in two distinct phylogenetic clusters and were flanked by samples from the older sampling time points with Bacteroidota (synonym Bacteroidetes) and Bacillota (syn. Firmicutes) becoming more dominant. Relative abundance of Actinomycetota (syn. Actinobacteria) was highly variable at early sampling time points and decreased with age (**Fig.**

2C). Gradual development of the infant microbiota is highlighted by increasing richness and alpha-diversity reaching significance at 3 months of age. Significant differences in average individual richness and Shannon effective number of species between infants and parents dissolved after 24 months (**Fig. 2D, Suppl. Fig. 2A**).

Unsupervised hierarchical clustering identified three distinct clusters across all infant samples during the first year of life (**Fig. 2E**). The clusters were characterized by a disproportionally high relative abundance (%) of the orders Bifidobacteriales (Cluster 1), Enterobacterales (Cluster 2) and Bacteroidales (Cluster 3) (**Fig. 2F**). Minor differences in bacterial abundance between the clusters included Eubacteriales (syn. Lachnospirales), Lactobacillales and Veillonellales-Selenomonadales (**Suppl. Fig. 2B**). The Bifidobacteriales-dominated cluster was enriched for breast-fed samples (adj. p-value = 0.003) and largely composed of fecal samples from early time points (7 and 12 months underrepresented, adj. p-value = 0.0004 and 3.904e-15, respectively). Formula consumption peaked at 3 months of age and breast-feeding simultaneously decreased with increasing formula milk consumption (**Fig. 2G**). Concordant with decreasing formula intake after 3 months (**Fig. 2G**), 97.5% of infants received solid foods by month 7 (**Table 1**). The two other clusters also included samples from older infants (7 and 12 months) (**Fig. 2H**). Samples from interventions and breast-fed infants (**Fig. 2H**) were equally present in clusters 2 and 3. In addition, fecal samples from babies born via C-section were overrepresented in cluster 2 (adj. p-value = 1.072e-18), and those born vaginally in cluster 3 (adj. p-value = 3.512e-19) (**Suppl. Fig. 2C**).

To define the impact of delivery and feeding modes on transmitted bacterial taxa from mothers to infants, we calculated the ratio of bacterial transmission between the mother-child dyads ordered by type of birth and feeding group. We defined this ratio as the number of shared zOTUs between the mother and the child divided by the total number of zOTUs present in the mother. We observed an increasing trend in the transmissibility over time during the 1st year (Kruskal Wallis p = 2.2e-16, **Suppl. Fig. 2D**). While for each individual time point, the type of feeding (feed groups A to D) did not significantly influence the bacterial transmissibility (data not shown), transmissibility was different between feed groups for all time points combined (p =0.00063). A post-hoc Dunn test showed that BF was significantly different to formula A and B in the 1st year of life (**Suppl. Fig. 2D**). The type of birth significantly affected the bacterial transmission in the 1st year (p = 0.0037). As previously shown[35], C-section birth altered bacterial transmission from mother at early age (months 0.5 and 1) but this trend was not significant at later time points (months 3, 7 and 12) (**Suppl. Fig. 2E**).

Impact of bifidobacterial and GOS intervention on infant microbiota assembly

Generalized UniFrac distance showed no significant differences between community structures of the four differentially supplemented infant formulas (A-D) and the exclusively breast-fed group (**Fig. 3A**), suggesting that inter-individual variations largely trumped the stratification of microbiota profiles based on feeding regiments. Species richness increased equally across feeding groups as infants aged (**Fig. 3B**). Beta-diversity was not significantly different between breast-feeders and the formula groups (**Suppl. Fig. 3A),** but differed between the placebo (Formula A) and other supplemented groups at age 3 months (**Suppl. Fig. 3B)**. No differences were seen at 24-months (**Suppl. Fig. 3C**). Beta-diversity was significantly different between babies born vaginally vs. by C-section especially at early age (0.5 and 1 months; **Suppl. Fig. 3D**). Progression in relative abundance of the top ten taxa over time are summarized in the horizon blot (**Fig. 3C**). *Bifidobacterium* was the most abundant genus (41.2%) across all infant fecal samples reaching peak abundance at the age of 3 months (**Fig. 3C**). Average abundance

169 of *Bifidobacterium* was lowest in the placebo group A (32.3%) followed by the bifidobacteria-
170 supplemented group B (39.7%). *Bacteroides, Escherichia-Shigella*, *Veillonella, Klebsiella,*
171 *Clostridium, Streptococcus* and *Enterococcus* contribute to the very early life infant
172 communities (months 0.5, 1, 3) at substantially lower abundance levels (<13%) (**Fig. 3C**).
173 Relative to the taxon median, the genera *Bacteroides* and *Blautia* clearly increased in average
174 abundance at month 7 and 12 (**Fig. 3C**). Despite some variation over time, formula-fed infants
175 showed on average a 29% higher abundance of *Veillonella* compared to breast-fed infants (**Fig.**
176 **3C**). GOS supplementation in the interventional groups C and group D (*Bifidobacterium* and
177 GOS) significantly increased the average bifidobacterial abundance compared to the control
178 group A at month 3 and 7 of age (low formula consumers omitted, **Fig. 3D**) but formula
179 supplementation with *B. longum* and *B. breve* (group B) failed to increase it. The comparison
180 of bifidobacterial abundances between breast-fed and formula fed-infants (low formula
181 consumers omitted) showed a complete loss of significance between any of the interventional
182 groups at 3 months, demonstrating that the inherent variability between samples is higher than
183 the effect of the intervention at this time point. At 7 months, significance of the GOS-mediated
184 effects on increased bifidobacterial abundance was maintained, suggesting that time of
185 exposure to formula supplements is important to sustain effects (data not shown). No additional
186 differences were detected between interventions (data not shown). Shallow metagenomic
187 analysis identified *B. longum*, *B. breve*, *V. parvula*, *E. coli* and *B. bifidum* as the 5 most abundant
188 and prevalent bacterial species at month 3 and 7 independent of the feeding groups (**Fig. 3E**).
189 Some breast-fed infants lacked the most common *Bifidobacterium* strains and instead harbored
190 different *Veillonella* species and *Enterococcus faecalis* (**Fig. 3E**). Correlation analysis based on
191 shallow metagenomics identified pathways related to amino acid biosynthesis (yellow boxes),
192 nucleoside and nucleotide biosynthesis (blue), cell structure biosynthesis (green) and cofactor,
193 carrier and vitamin biosynthesis (orange) in decreasing abundance (**Fig. 3F**). In accordance
194 with the low fiber availability at these early life stages, fermentation was the least abundant
195 pathway. No clear clustering occurred in relation to age and feeding (**Fig. 3F**).

196 **Metabolites clearly differ between feeding groups and display diurnal rhythmicity**

197 We next characterized the metabolite milieu at three months of age since solid food has not
198 been introduced yet and infants consumed the highest volume of formula at this time point.
199 Principal Component Analysis (PCA) identified significantly separated clusters for breast-fed
200 and formula-fed infants, while formula-fed infants remained indistinguishable (**Fig. 4A**, left
201 blot). Interestingly, the exclusively formula-fed infants clustered away from the breast-fed
202 infants, while the mixed feeding (receiving breastmilk and formula) partially overlapped with
203 the breast-fed infants (**Fig. 4A**, right blot), suggesting that the intake of either breastmilk or
204 infant formula plays a significant role in the respective fecal metabolic profiles. To further
205 resolve the metabolome differences between breast-fed and formula-fed infants, we performed
206 additional analyses (PCA) of metabolite profiles from human and formula milk, including 103
207 breastmilk samples and the 4 different formulas. Here, we demonstrated that formula samples
208 clearly cluster away from all breastmilk samples (**Suppl. Fig. 1D**). Furthermore, breastmilk
209 samples separated in two distinct clusters which equally distribute across all fecal samples
210 (**Suppl. Fig. 1E**), suggesting that the difference in the breastmilk metabolome are not
211 exclusively responsible for the differences in the fecal metabolome.

212 Cluster analysis of metabolite abundances was used to stratify patterns according to the feeding
213 groups (**Fig. 4B**). As illustrated in the heatmap for the 49 most abundant features, breast- and
214 formula-fed infants differentially clustered with only occasional appearance of samples from

formula-fed infants in the breast-fed cluster (**Fig. 4B**). A more detailed analysis on the respective metabolites, phosphocholines as well as some specialized sugar derivatives like sugar acid, N-acetylated quadruple sugar or N-acetylated trisaccharide are increased in the breast-fed group, whereas carnitines is increased in all formula-fed groups. Indole derivatives such as bacterial-derived indolelactic acid is also increased in formula-fed groups B, C and D (**Fig. 4C**). Network correlational analysis was employed to identify the association of bacterial species and fecal metabolites (**Fig. 4D**). The top ten significantly bacterial species correlated positively or negatively with metabolites, suggesting functional redundancy between taxa (**Fig. 4E**). Variation in abundance of metabolites and bacteria according to the sampling daytime was previously identified in adult populations[27,28]. To evaluate whether this also occurs in infants in the first year of life, we analyzed daytime-dependent fluctuations in metabolite abundance at age 3 months. Peak abundance of fecal metabolites across all fecal samples is illustrated in the heatmap, supporting diurnal rhythms (**Fig. 4F**). Rhythmic metabolites appeared different depending on each feed and birth mode but maintained rhythms (**Suppl. Fig. 4A, B**). Network correlational analysis further correlated bacteria (zOTUs), such as *B. longum* and *Veillonella* and rhythmic metabolites (**Fig. 4G**). These findings support the hypothesis that circadian regulation starts at early stages of life with possible functional contribution to the infant microbiome.

The development of diurnal rhythmicity of the infant microbiota is affected by age and formula supplementation

In accordance to daytime-dependent differences in metabolite abundance and their link to distinct bacterial taxa (**Fig. 4G**), significant diurnal rhythms were found in bacterial richness and alpha-diversity of fecal samples collected from infants throughout day and night (**Fig. 5A, Suppl. Fig. 4C, D**). Diurnal rhythmicity was also present at the level of individual zOTUs as illustrated by their normalized peak abundance across the 24 h day (**Fig. 5B**). Interestingly, significant rhythmicity was detected for the highly abundant genera *Bifidobacterium* (**Fig. 5C**). The amount of diurnal zOTUs increased as infants mature in parallel to the increasing diversification of infant gut microbiota, with highest numbers of rhythmic zOTUs at age 12 months (**Fig. 5D**). Of note, rhythmic zOTUs were most numerous in cluster 3 containing samples of older infants (**Fig. 2H, Suppl. Fig. 4E**). Rhythmic zOTUs were detected dependent on the birth types (**Suppl. Fig. 4F**). Interestingly, the number of rhythmic bacteria was highest in formula groups supplemented with bifidobacteria and GOS, which even exceeded the number of rhythmic zOTUs in breast-fed infants (**Fig. 5E**). Independent of the groups, the highest numbers of rhythmic zOTUs belonged to the genera *Veillonella* (7 zOTUs), *Bacteroides* (6 zOTUs), *Bifidobacterium* (6 zOTUs), *Streptococcus* (6 zOTUs) and *Clostridium* (5 zOTUs). PICRUSt2 analysis revealed that the total amount of significantly rhythmic assigned pathways dominated in samples from formula group D at age 7 months (604), followed by the breast-fed group showing rhythmicity in 162 pathways (**Fig. 5F**). Furthermore, LEfSe analysis[36] of these rhythmic metabolic pathways identified that the placebo group (formula A) differed the most from the other feeding groups and particularly 29 rhythmic pathways differed between placebo and breast-fed infants (**Suppl. Fig. 4G**). Interestingly, in all group-to-placebo comparisons, fatty acid beta-degradation was enriched in placebo-fed infants (**Suppl. Fig. 4G**). In contrast to the placebo group, results from the groups supplemented with formula containing bifidobacteria and GOS most closely resembled the breast-fed group.

Circadian rhythms in dominant infant microbial taxa persist *in vitro*

In order to investigate whether microbial rhythms observed during early life are host-driven or rely on microbial intrinsic clock mechanisms, fecal samples from selected exclusive breast-fed and formula-fed (group A) infants at age 3 months were cultured in a chemostat model. To establish stable growth conditions, an initial adaptation phase (batch culture) was set up followed by continuous culturing for 7 days in the chemostat to ensure host-independent conditions (**Fig. 5G**). Beta diversity was similar between chemostats containing stool samples from the breast-fed donor, but differed significantly between feeding conditions (**Suppl. Fig. 5A**). In contrast to the inoculum, which was highly enriched in *Bifidobacterium* (>90% abundance) in the breast-fed sample, *Bifidobacterium* reached notably lower average abundance in the chemostat (12.79 < 89.73 in breast-fed; 4.74 < 75.49 in group A) (**Suppl. Fig. 5B**). In the second paired chemostat, the inoculum came from placebo formula group A, and the genera *Clostridium* and *Escherichia−Shigella* were similarly enriched, whereas *Bifidobacterium* was low in abundance (**Suppl. Fig. 5B)**. To investigate potential rhythmic alterations in abundance, beginning at day seven of continuous culture, samples were taken every 4 hours over the course of 48 hours (**Fig. 5G)**. Circadian analysis on microbiota composition revealed truly endogenous circadian rhythms in all chemostats illustrated at the level of dominant phyla, families and genera (**Fig 5H, Suppl. Fig. 5B, C**). Rhythmic changes in abundance are highlighted for highly abundant zOTUs (**Fig. 5I, Suppl. Fig. 5D**) and selected metabolic pathways (PICRUSt2 analysis, **Suppl. Fig. 5E**). In accordance with results demonstrated in infant stool samples (**Fig. 5C, E**), significant rhythms were identified for zOTUs of the genera *Bifidobacterium* and *Enterobacteriaceae,* which were overrepresented in the breast-fed samples, and *Clostridium sensu stricto* 1, which were overrepresented in chemostat samples from formula A (**Fig. 5I, Suppl. Fig. 5D**). These results are the first demonstration that specific taxa from a complex microbiota undergo circadian rhythmicity after seven days of continuous culture, pointing to a host-independent, intrinsic establishment of rhythmicity in the infant bacteria.

Discussion

In this randomized, controlled intervention trial, we demonstrated that formula- and breast-fed infants share characteristic features of microbiota assembly in the first year of life including age-related increase in bacterial richness and diversity as well as dominant abundance of specific bifidobacterial species. Interestingly 24-hour bacterial oscillations were present in all groups and could be integrated into rhythmic metabolite networks. Of note, bacterial profiles highly varied between individuals, even though the study population was homogenous related to geographical area, formula consumption, daily routines (sleep, eat, diaper change) as well as birth, family and health characteristics of the cohort. Interestingly, formula- and breast-fed infants substantially differed in their metabolite profiles, despite considerably overlapping bacterial community structures, emphasizing the unique composition of breast milk.[37] Nevertheless, and consistent with previous findings,[15,38,39] GOS supplemented infant formula was most efficient to sustain high levels of the genus *Bifidobacterium* compared to formula containing bifidobacteria or placebo. Remarkably, the presence of GOS in infant formula resulted in the high numbers of rhythmic zOTUs across a range of different bacterial taxa, even exceeding the number of rhythmic zOTUs in breastfed infants. Similar but less pronounced was the effect of formula supplementation with *B. longum* and *B. breve*, despite representing the most abundant species in the infant gut, however placebo showed the fewest number of rhythmic bacterial taxa. Host independent circadian regulation of bacterial rhythmicity was

305 confirmed in breast-fed and infant formula derived stool microbiota using an *ex vivo* gut
306 chemostat model. These findings demonstrate for the first time that bacterial intrinsic clock
307 mechanisms contribute to the development of circadian rhythmicity in the microbiota at early
308 life stages.

309 The infant microbiome gradually develops towards a more diverse adult-like microbiome over
310 time.[7] Interestingly, shallow metagenomics sequencing of samples from 3- and 7-months old
311 infants demonstrated that *Bifidobacterium* (*B. breve*, *B. longum* and *B. bifidum*), *Veillonella*
312 and *Enterobacteriaceae* dominate this early life stage, irrespective of the diet received. These
313 results are consistent with previously published baby cohort where fecal samples of 40 days, 3-
314 months and 6-months old infants were compared, showing that *Bifidobacterium* and
315 *Enterobacteriaceae* were the most predominant taxa, regardless of diet and age.[40] Alpha-
316 diversity significant increased from age 3 months onwards, gradually approaching parental
317 diversity levels at age 24 months. This is in line with previous reports indicating significant
318 changes in the dominant phyla and diversity appearing from age 3 months onwards[16] or at the
319 end of the first year of life[41] until the parent's diversity and composition is reached by month
320 14[16] or on the second birthday.[42] None of the three types of supplementation investigated in this
321 study were able to fully recreate the breast milk-related microbial environment. Accordingly,
322 the fecal metabolic profile of 3-months old, breast-fed babies was clearly distinguishable from
323 formula-consuming infants. Untargeted metabolomics of breastmilk and infant samples
324 identified clear differences in the metabolite profiles and considering the respective fecal
325 samples, we conclude that the intake of either breastmilk or infant formula plays a significant
326 role in shaping the fecal metabolome. Breast-fed babies showed a high number of organic
327 oxygen metabolites in their feces, whereas formula-fed babies were associated with a lipid-
328 enriched metabolome composition. Similarly, metabolic profiles of 12 month old infants were
329 reported to be distinguishable between diets.[43] In addition, the two distinct clusters of
330 metabolite profiles in breastmilk, which appeared at least in part to be differentiated by the
331 presence of the human milk oligosaccharide fucosyllactose, are not exclusively responsible for
332 the differences in the fecal metabolome.

333 Previous work in adult populations, done by others as well as our group, documented that
334 microbiota composition and function undergoes diurnal rhythmicity.[26,44] However, whether
335 these rhythms appear at early age remained unknown. We provide the first evidence that during
336 the first year of life in all feeding groups, the abundance of the most dominant taxa, including
337 *Bifidobacterium*, varied depending on the time of defecation and circadian rhythm analysis
338 revealed that these fluctuations follow the 24-hour day. These diurnal oscillations could indeed
339 explain the opposing results on abundance fluctuations reported, e.g. for bifidobacteria[45] if
340 samples were taken at different day times in previous studies. Here we discovered significant
341 daytime-dependent fluctuations in bacterial diversity, at the level of genera and zOTUs in infant
342 stool samples. Although rhythmicity was present in all feeding groups and at all ages examined,
343 including the genera *Veillonella*, *Bacteroides*, *Bifidobacterium*, *Streptococcus* and *Clostridium*,
344 dramatic differences were detected between rhythmic zOTUs based on infant, age and diet. The
345 overall highest number of rhythmic zOTUs was found in infants fed with formula supplemented
346 with the combination of bifidobacteria and GOS, which exceeded numbers seen in breast-fed
347 infants. Moreover, circadian analysis identified the presence of diurnal rhythms in microbiota
348 composition and function already in 2-weeks old infants demonstrating that microbial
349 oscillations are an early event in the infant gut development. The number of rhythmic bacteria

gradually increased as the infant gut matured and regular diet was introduced to the infant nutrition.

Circadian regulation of microbiota composition and function was recently shown to depend on the host circadian clock, particularly in intestinal epithelial cells.[46] Conversely, microbiota have been shown to influence host circadian rhythms,[47,48] indicating a cross-talk between the host interface and bacteria. Microbiota transfer experiments further demonstrated the physiological relevance of microbial oscillations for the host's metabolic and gastrointestinal health.[26,46,49] Since environmental factors, such as the light-dark-cycle, or time of food intake, are potent signals impacting microbial rhythms,[26,46,49,50] abnormal light or food exposure can alter microbial oscillations and thus might lead to the development of pathologies and disease. To gain further insights into the possible functionality of microbiota oscillations in infants, rhythmic zOTU-associated pathways were examined. Similar to results obtained from the taxonomic analysis, most rhythmic assigned pathways were found in 3- and 7-months old infants fed with formula containing GOS or both the prebiotic supplement and bifidobacteria respectively, followed by breast-fed infants. Importantly, results from the placebo group differed the most from breast-fed infants, whereas results from infants fed with formula containing bifidobacteria and GOS most closely resembled the breast-fed group. The association between the bifidogenic effect of GOS supplementation and the augmentation of the number of rhythmic pathways needs to be further investigated in future studies.

Recent work on single bacterial cultures discovered rhythmic gene expression in *Bacillus subtilis*[24] and recorded circadian rhythms in the swarming behavior of the gut bacterium *Klebsiella aerogenes*[25]. To identify whether the diurnal rhythms observed in infants gut microbiota are generated by the host circadian clock or bacterial intrinsic mechanism, we cultured complex microbiota communities in a chemostat model. For this purpose, samples from either exclusively breastfed or formula A-fed infants were cultured and supplemented with media containing infant formula. Of note, the relative abundance of taxa as well as bacterial diversity changed significantly when compared to the original inoculum. Despite both inocula being dominated by bifidobacteria, their relative abundance decreased after the continuous flow with culture media begun until a fluctuating but steady abundance was achieved. Importantly, after 7 days *in vitro* when the communities were established, circadian rhythm analysis of microbiota composition provides the first evidence of circadian rhythms in the abundance of dominant bacteria, such as *Bifidobacterium*, *Veillonella*, *Clostridium* and *Bacteroides*, in complex human microbiota communities. Since oscillations from 3-months old infant stool samples are documented outside and independent of the host, these are truly endogenous circadian rhythms and therefore must be generated by bacterial intrinsic clock mechanisms. Importantly, we observed that rhythmic bacterial taxa differed depending on whether the original sample was obtained from an exclusively breastfed infant or exclusively fed with formula A. For example, the composition of breast-fed infants was dominated by rhythmic oscillations of zOTUs belonging to *Enterobacteriacea* and *Bifidobacterium*, whereas formula A-fed samples were enriched with rhythmic zOTUs belonging to *Clostridium* and *Bacteroides.* However, independent of which taxa dominated in both extreme infant feeding exposures (exclusive BF and exclusive formula A), all of them had the potential to become rhythmic *in vitro*, suggesting the importance of bacterial intrinsic clock mechanism for the establishment of circadian microbial communities in the developing infant gut.

Possible limitations of the circadian analysis include the fact that the number of fecal samples collected during the night is lower compared to daytimes and decreases with age. This possibly

results from the reluctance of parents to sample feces at night, but also shows the adaptation of older infants to the rhythms of their parents. In any case, the statistical model reached significance even with reduced sample numbers emphasizing the robust finding that distinct taxa of the infant microbiota develop circadian rhythms at early life stages. Furthermore, the explicit contribution of breastmilk relative to infant formula on bacterial rhythms remains unclear, since breastfeeding being the official recommended diet for infants was advocated, and consequently, the group size for exclusively formula-fed infants was limited. Finally, the *ex-vivo* chemostat model allowed us to replicate the infant colonic environment to some extent and to identify bacterial rhythms independent of the host. However, the composition of the infant microbiota was not fully recovered in the chemostat model, suggesting that we only identified an incomplete repertoire of rhythmic taxa. Mechanisms explaining endogenous triggers for bacterial rhythms, such as circadian clock genes, are still missing and will be further investigated.

In summary, this controlled intervention study provided compelling evidence of circadian rhythmicity in the developing infant gut microbiota affected by diet. Our findings warrant the need for further analysis of circadian fluctuations of both bacteria and metabolites and their functional role in contributing to the benefits of infant nutrition.

References

1. Martino, C., Dilmore, A.H., Burcham, Z.M., Metcalf, J.L., Jeste, D., and Knight, R. (2022). Microbiota succession throughout life from the cradle to the grave. Nature Reviews Microbiology *20*, 707-720.
2. Penders, J., Thijs, C., Vink, C., Stelma, F.F., Snijders, B., Kummeling, I., van den Brandt, P.A., and Stobberingh, E.E. (2006). Factors influencing the composition of the intestinal microbiota in early infancy. Pediatrics *118*, 511-521.
3. Ferretti, P., Pasolli, E., Tett, A., Asnicar, F., Gorfer, V., Fedi, S., Armanini, F., Truong, D.T., Manara, S., and Zolfo, M. (2018). Mother-to-infant microbial transmission from different body sites shapes the developing infant gut microbiome. Cell host & microbe *24*, 133-145. e135.
4. Yang, I., Corwin, E.J., Brennan, P.A., Jordan, S., Murphy, J.R., and Dunlop, A. (2016). The infant microbiome: implications for infant health and neurocognitive development. Nursing research *65*, 76.
5. Al Nabhani, Z., and Eberl, G. (2020). Imprinting of the immune system by the microbiota early in life. Mucosal immunology *13*, 183-189.
6. Mueller, N.T., Bakacs, E., Combellick, J., Grigoryan, Z., and Dominguez-Bello, M.G. (2015). The infant microbiome development: mom matters. Trends in molecular medicine *21*, 109-117.
7. Bäckhed, F., Roswall, J., Peng, Y., Feng, Q., Jia, H., Kovatcheva-Datchary, P., Li, Y., Xia, Y., Xie, H., and Zhong, H. (2015). Dynamics and stabilization of the human gut microbiome during the first year of life. Cell host & microbe *17*, 690-703.
8. Milani, C., Duranti, S., Bottacini, F., Casey, E., Turroni, F., Mahony, J., Belzer, C., Palacio, S.D., Montes, S.A., and Mancabelli, L. (2017). The first microbial colonizers of the human gut: composition, activities, and health implications of the infant gut microbiota. Microbiology and Molecular Biology Reviews *81*.
9. Lawson, M.A., O'Neill, I.J., Kujawska, M., Gowrinadh Javvadi, S., Wijeyesekera, A., Flegg, Z., Chalklen, L., and Hall, L.J. (2020). Breast milk-derived human milk oligosaccharides promote Bifidobacterium interactions within a single ecosystem. The ISME journal *14*, 635-648.
10. Bazanella, M., Maier, T.V., Clavel, T., Lagkouvardos, I., Lucio, M., Maldonado-Gòmez, M.X., Autran, C., Walter, J., Bode, L., and Schmitt-Kopplin, P. (2017). Randomized controlled trial

445 on the impact of early-life intervention with bifidobacteria on the healthy infant fecal microbiota
446 and metabolome. The American journal of clinical nutrition *106*, 1274-1286.
447 11. Bode, L. (2012). Human milk oligosaccharides: every baby needs a sugar mama. Glycobiology
448 *22*, 1147-1162.
449 12. Ballard, O., and Morrow, A.L. (2013). Human milk composition: nutrients and bioactive
450 factors. Pediatric Clinics of North America *60*, 49-74.
451 13. Bode, L., and Jantscher-Krenn, E. (2012). Structure-function relationships of human milk
452 oligosaccharides. Advances in Nutrition *3*, 383S-391S.
453 14. Veereman-Wauters, G., Staelens, S., Van de Broek, H., Plaskie, K., Wesling, F., Roger, L.,
454 McCartney, A., and Assam, P. (2011). Physiological and bifidogenic effects of prebiotic
455 supplements in infant formulae. Journal of pediatric gastroenterology and nutrition *52*, 763-771.
456 15. Sierra, C., Bernal, M.-J., Blasco, J., Martínez, R., Dalmau, J., Ortuno, I., Espín, B., Vasallo, M.-
457 I., Gil, D., and Vidal, M.-L. (2015). Prebiotic effect during the first year of life in healthy infants
458 fed formula containing GOS as the only prebiotic: a multicentre, randomised, double-blind and
459 placebo-controlled trial. European journal of nutrition *54*, 89-99.
460 16. Stewart, C.J., Ajami, N.J., O'Brien, J.L., Hutchinson, D.S., Smith, D.P., Wong, M.C., Ross,
461 M.C., Lloyd, R.E., Doddapaneni, H., and Metcalf, G.A. (2018). Temporal development of the
462 gut microbiome in early childhood from the TEDDY study. Nature *562*, 583-588.
463 17. Cox, L.M., Yamanishi, S., Sohn, J., Alekseyenko, A.V., Leung, J.M., Cho, I., Kim, S.G., Li, H.,
464 Gao, Z., and Mahana, D. (2014). Altering the intestinal microbiota during a critical
465 developmental window has lasting metabolic consequences. Cell *158*, 705-721.
466 18. Vandenplas, Y., Greef, E.D., and Veereman, G. (2014). Prebiotics in infant formula. Gut
467 microbes *5*, 681-687.
468 19. Mugambi, M.N., Musekiwa, A., Lombard, M., Young, T., and Blaauw, R. (2012). Synbiotics,
469 probiotics or prebiotics in infant formula for full term infants: a systematic review. Nutrition
470 journal *11*, 1-32.
471 20. Indrio, F., Gutierrez Castrellon, P., Vandenplas, Y., Cagri Dinleyici, E., Francavilla, R.,
472 Mantovani, M.P., Grillo, A., Beghetti, I., Corvaglia, L., and Aceti, A. (2022). Health Effects of
473 Infant Formula Supplemented with Probiotics or Synbiotics in Infants and Toddlers: Systematic
474 Review with Network Meta-Analysis. Nutrients *14*, 5175.
475 21. Braegger, C., Chmielewska, A., Decsi, T., Kolacek, S., Mihatsch, W., Moreno, L., Piescik, M.,
476 Puntis, J., Shamir, R., and Szajewska, H. (2011). Supplementation of infant formula with
477 probiotics and/or prebiotics: a systematic review and comment by the ESPGHAN committee on
478 nutrition. Journal of pediatric gastroenterology and nutrition *52*, 238-250.
479 22. Mohawk, J.A., Green, C.B., and Takahashi, J.S. (2012). Central and peripheral circadian clocks
480 in mammals. Annu Rev Neurosci *35*, 445-462. 10.1146/annurev-neuro-060909-153128.
481 23. Roenneberg, T., and Merrow, M. (2016). The circadian clock and human health. Current biology
482 *26*, R432-R443.
483 24. Eelderink-Chen, Z., Bosman, J., Sartor, F., Dodd, A.N., Kovacs, A.T., and Merrow, M. (2021).
484 A circadian clock in a nonphotosynthetic prokaryote. Sci Adv *7*. 10.1126/sciadv.abe2086.
485 25. Paulose, J.K., Cassone, C.V., Graniczkowska, K.B., and Cassone, V.M. (2019). Entrainment of
486 the Circadian Clock of the Enteric Bacterium Klebsiella aerogenes by Temperature Cycles.
487 iScience *19*, 1202-1213. 10.1016/j.isci.2019.09.007.
488 26. Thaiss, C.A., Zeevi, D., Levy, M., Zilberman-Schapira, G., Suez, J., Tengeler, A.C., Abramson,
489 L., Katz, M.N., Korem, T., and Zmora, N. (2014). Transkingdom control of microbiota diurnal
490 oscillations promotes metabolic homeostasis. Cell *159*, 514-529.
491 27. Reitmeier, S., Kiessling, S., Clavel, T., List, M., Almeida, E.L., Ghosh, T.S., Neuhaus, K.,
492 Grallert, H., Linseisen, J., Skurk, T., et al. (2020). Arrhythmic Gut Microbiome Signatures
493 Predict Risk of Type 2 Diabetes. Cell Host Microbe *28*, 258-272 e256.
494 10.1016/j.chom.2020.06.004.
495 28. Thaiss, C.A., Zeevi, D., Levy, M., Zilberman-Schapira, G., Suez, J., Tengeler, A.C., Abramson,
496 L., Katz, M.N., Korem, T., Zmora, N., et al. (2014). Transkingdom control of microbiota diurnal
497 oscillations promotes metabolic homeostasis. Cell *159*, 514-529. 10.1016/j.cell.2014.09.048.
498 29. Liang, X., Bushman, F.D., and FitzGerald, G.A. (2015). Rhythmicity of the intestinal
499 microbiota is regulated by gender and the host circadian clock. Proc Natl Acad Sci U S A *112*,
500 10479-10484. 10.1073/pnas.1501305112.

30. Altaha, B., Heddes, M., Pilorz, V., Niu, Y., Gorbunova, E., Gigl, M., Kleigrewe, K., Oster, H., Haller, D., and Kiessling, S. (2022). Genetic and environmental circadian disruption induce weight gain through changes in the gut microbiome. Mol Metab *66*, 101628. 10.1016/j.molmet.2022.101628.
31. Heddes, M., Altaha, B., Niu, Y., Reitmeier, S., Kleigrewe, K., Haller, D., and Kiessling, S. (2022). The intestinal clock drives the microbiome to maintain gastrointestinal homeostasis. Nat Commun *13*, 6068. 10.1038/s41467-022-33609-x.
32. Escobar, C., Rojas-Granados, A., and Angeles-Castellanos, M. (2021). Development of the circadian system and relevance of periodic signals for neonatal development. Handb Clin Neurol *179*, 249-258. 10.1016/B978-0-12-819975-6.00015-7.
33. Mukherji, A., Kobiita, A., Ye, T., and Chambon, P. (2013). Homeostasis in intestinal epithelium is orchestrated by the circadian clock and microbiota cues transduced by TLRs. Cell *153*, 812-827. 10.1016/j.cell.2013.04.020.
34. Leone, V., Gibbons, S.M., Martinez, K., Hutchison, A.L., Huang, E.Y., Cham, C.M., Pierre, J.F., Heneghan, A.F., Nadimpalli, A., Hubert, N., et al. (2015). Effects of diurnal variation of gut microbes and high-fat feeding on host circadian clock function and metabolism. Cell Host Microbe *17*, 681-689. 10.1016/j.chom.2015.03.006.
35. Boned-Rico, L., Martín-Martín, R., and Albiach-Benito, C. (2023). Siembra vaginal para enriquecer el microbioma de los bebés nacidos por cesárea: revisión de casos. Paraninfo Digital, e35036d-e35036d.
36. Segata, N., Izard, J., Waldron, L., Gevers, D., Miropolsky, L., Garrett, W.S., and Huttenhower, C. (2011). Metagenomic biomarker discovery and explanation. Genome biology *12*, 1-18.
37. Andreas, N.J., Kampmann, B., and Le-Doare, K.M. (2015). Human breast milk: A review on its composition and bioactivity. Early human development *91*, 629-635.
38. Ben, X.-M., Li, J., Feng, Z.-T., Shi, S.-Y., Lu, Y.-D., Chen, R., and Zhou, X.-Y. (2008). Low level of galacto-oligosaccharide in infant formula stimulates growth of intestinal Bifidobacteria and Lactobacilli. World journal of gastroenterology: WJG *14*, 6564.
39. Matsuki, T., Tajima, S., Hara, T., Yahagi, K., Ogawa, E., and Kodama, H. (2016). Infant formula with galacto-oligosaccharides (OM55N) stimulates the growth of indigenous bifidobacteria in healthy term infants. Beneficial microbes *7*, 453-461.
40. Ma, J., Li, Z., Zhang, W., Zhang, C., Zhang, Y., Mei, H., Zhuo, N., Wang, H., Wang, L., and Wu, D. (2020). Comparison of gut microbiota in exclusively breast-fed and formula-fed babies: A study of 91 term infants. Scientific Reports *10*, 15792.
41. Clemente, J.C., Ursell, L.K., Parfrey, L.W., and Knight, R. (2012). The impact of the gut microbiota on human health: an integrative view. Cell *148*, 1258-1270.
42. Wernroth, M.-L., Peura, S., Hedman, A.M., Hetty, S., Vicenzi, S., Kennedy, B., Fall, K., Svennblad, B., Andolf, E., and Pershagen, G. (2022). Development of gut microbiota during the first 2 years of life. Scientific Reports *12*, 9080.
43. Sillner, N., Walker, A., Lucio, M., Maier, T.V., Bazanella, M., Rychlik, M., Haller, D., and Schmitt-Kopplin, P. (2021). Longitudinal profiles of dietary and microbial metabolites in formula-and breastfed infants. Frontiers in Molecular Biosciences *8*, 660456.
44. Reitmeier, S., Kiessling, S., Clavel, T., List, M., Almeida, E.L., Ghosh, T.S., Neuhaus, K., Grallert, H., Linseisen, J., and Skurk, T. (2020). Arrhythmic gut microbiome signatures predict risk of type 2 diabetes. Cell host & microbe *28*, 258-272. e256.
45. Taft, D.H., Liu, J., Maldonado-Gomez, M.X., Akre, S., Huda, M.N., Ahmad, S., Stephensen, C.B., and Mills, D.A. (2018). Bifidobacterial dominance of the gut in early life and acquisition of antimicrobial resistance. Msphere *3*, e00441-00418.
46. Heddes, M., Altaha, B., Niu, Y., Reitmeier, S., Kleigrewe, K., Haller, D., and Kiessling, S. (2022). The intestinal clock drives the microbiome to maintain gastrointestinal homeostasis. Nature Communications *13*, 6068.
47. Brooks, J.F., Behrendt, C.L., Ruhn, K.A., Lee, S., Raj, P., Takahashi, J.S., and Hooper, L.V. (2021). The microbiota coordinates diurnal rhythms in innate immunity with the circadian clock. Cell *184*, 4154-4167. e4112.
48. Mukherji, A., Kobiita, A., Ye, T., and Chambon, P. (2013). Homeostasis in intestinal epithelium is orchestrated by the circadian clock and microbiota cues transduced by TLRs. Cell *153*, 812-827.

557 49. Altaha, B., Heddes, M., Pilorz, V., Niu, Y., Gorbunova, E., Gigl, M., Kleigrewe, K., Oster, H.,
558 Haller, D., and Kiessling, S. (2022). Genetic and environmental circadian disruption induce
559 weight gain through changes in the gut microbiome. Molecular Metabolism *66*, 101628.
560 50. Voigt, R.M., Forsyth, C.B., Green, S.J., Mutlu, E., Engen, P., Vitaterna, M.H., Turek, F.W., and
561 Keshavarzian, A. (2014). Circadian disorganization alters intestinal microbiota. PloS one *9*,
562 e97500.

563

Additional information

Corresponding author

Correspondence to Prof. Dr. Dirk Haller, Chair of Nutrition and Immunology, Technical University of Munich, Gregor-Mendel-Str. 2, 85354 Freising, Germany; dirk.haller@tum.de

Acknowledgements

The Infantibio-II study was initiated and financed by Töpfer GmbH (Dietmannsried, Germany). Besides manufacturing the study formula, they had no role in the conduct and management of the study, analysis and interpretation of data nor the creation of this manuscript. D.H. and S.K. received funding from the German Research Foundation (DFG, Deutsche Forschungsgemeinschaft) SFB 1371 (no. 395357507). D.H. also received funding in the frame of the Joint Programming Initiative of the European Union (project name EcoBiotic) and the German Ministry of Education and Research (BMBF; FKZ 01EA2207). The Technical University of Munich provided technical support through the Core Facility Microbiome of the ZIEL Institute for Food & Health (Klaus Neuhaus, Lukas Mix, Angela Sachsenhauser and Caroline Ziegler) for 16S rRNA gene amplicon sequencing. We thank Nikolai Köhler for giving us advice on integrative data analysis as well as Katharina Sontheimer, Claudia Seegerer and Franziska Kummert for support with sample management and handling. We are most grateful to the participating families and infants of the Infantibio-II study for their time, effort and enthusiasm in our study.

Author contributions

D.H. conceived and coordinated the project and secured funding. S.K. performed and supervised the circadian analysis. N.H. and D.H. were responsible for creation of trial documents and ethics approval, N.H. was responsible for participant recruitment, enrolment, data collection, management and coordination of collection of all trial samples. N.H., S.R., H.O., S.K. and M.VM. performed 16S rRNA sequencing and subsequent analysis with support from L.S. and M.L., and M.G., S.R. C.M. and K.K. were responsible for metabolomics analysis. S.R. and M.S. performed shotgun metagenomics analysis, H.O., M.H. and M.VM. performed the chemostat experiments and analysis, N.H., S.R., and M.L. performed bioinformatics analysis. D.H., S.K. and H.O. supervised the work and data analysis. N.H., S.K. and D.H. wrote the manuscript. All authors reviewed the manuscript.

Competing interest declaration

The authors declare no competing interests.

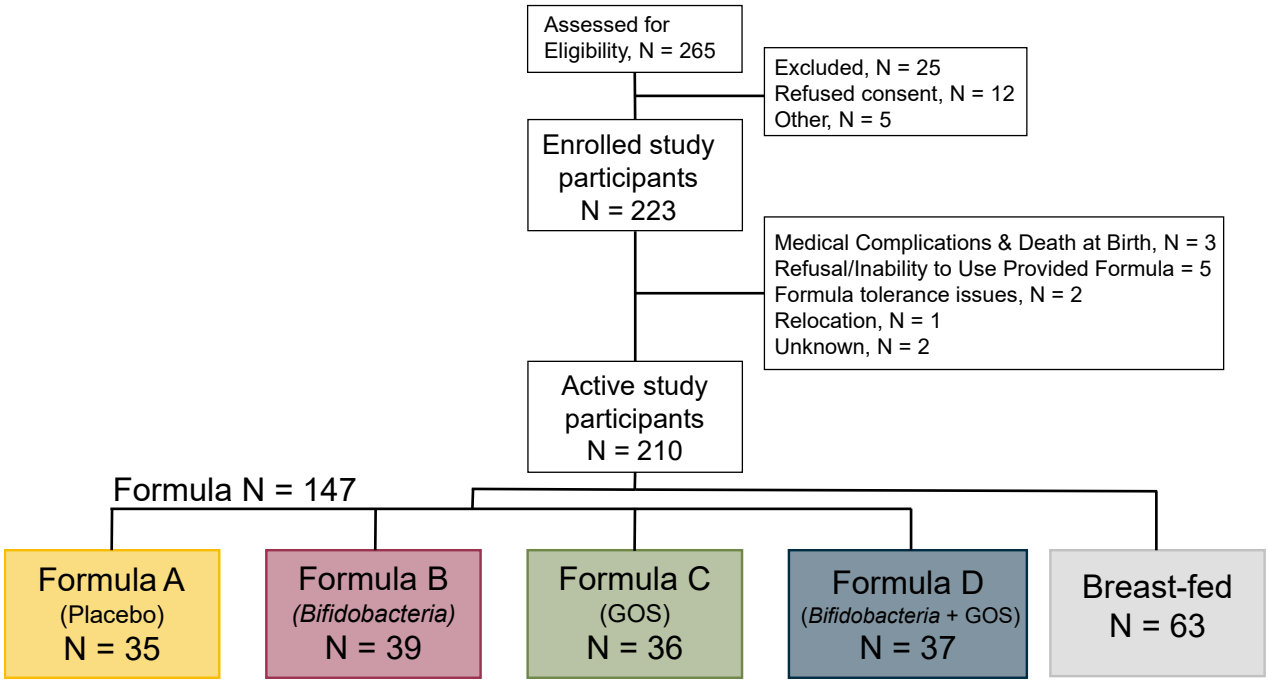
Assessed for Eligibility, N = 265
Excluded, N = 25
Refused consent, N = 12
Other, N = 5
Enrolled study participants N = 223
Medical Complications & Death at Birth, N = 3
Refusal/Inability to Use Provided Formula = 5
Formula tolerance issues, N = 2
Relocation, N = 1
Unknown, N = 2
Active study participants N = 210
Formula N = 147
Formula A (Placebo) N = 35
Formula B (Bifidobacteria) N = 39
Formula C (GOS) N = 36
Formula D (Bifidobacteria + GOS) N = 37
Breast-fed N = 63

596 **Figure 1 Study schematic of participant enrollment and randomization.**
597 Schematic of participant enrolment and reasons for drop-out before start of study. Active study
598 participants (N =210), provided at least one fecal sample. Newborns were randomly assigned
599 to one of four formula groups: Placebo, *Bifidobacterium*-supplemented (Formula B), galacto-
600 oligosaccharide (GOS)-supplemented (Formula C) or formula containing GOS and
601 *Bifidobacteria* (Formula D). Breast-fed infants that never consumed any of the provided
602 formula served as reference group.

603

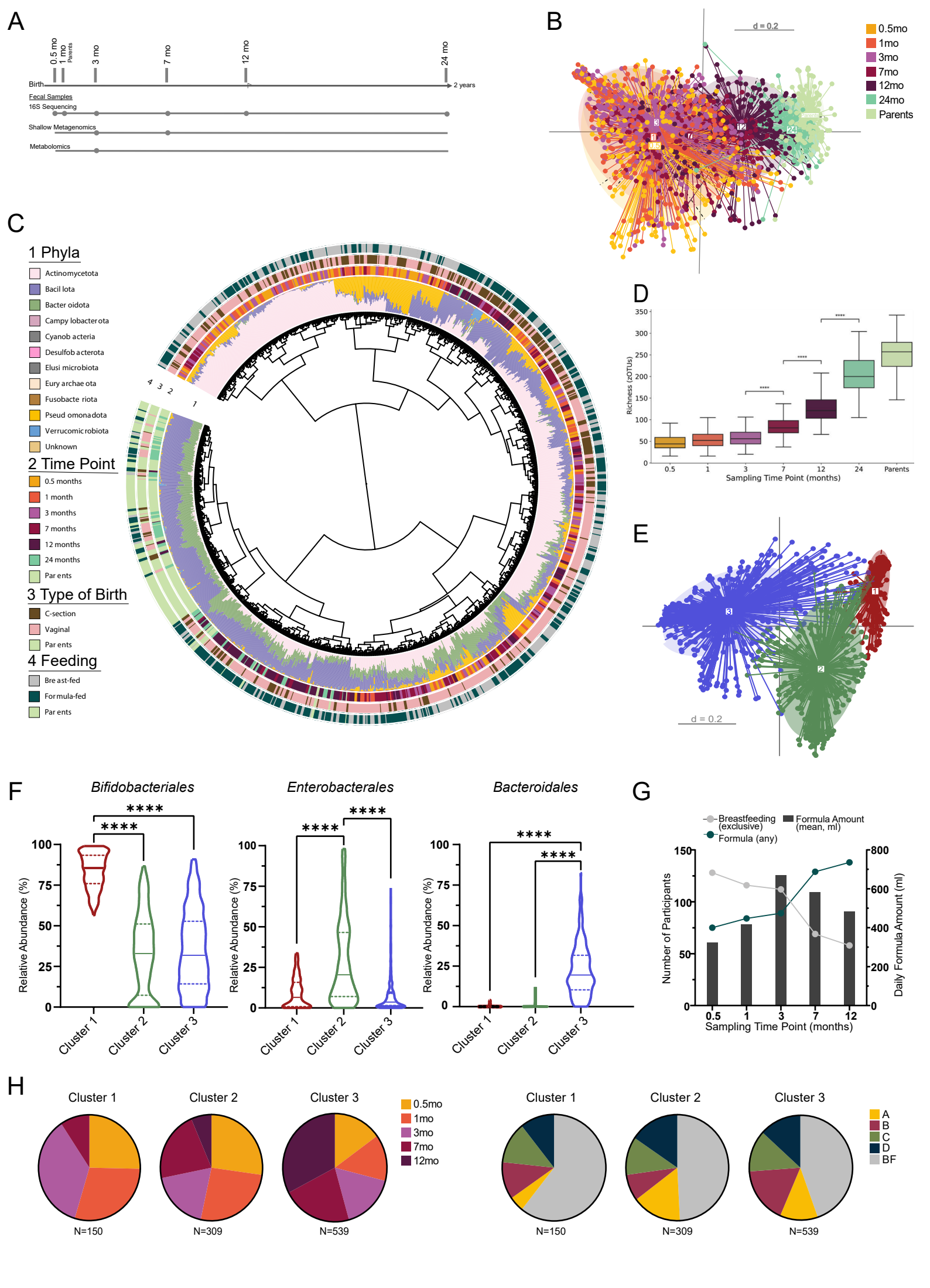
A
0.5 mo
1 mo
Parents
3 mo
7 mo
12 mo
24 mo
Birth
2 years
Fecal Samples
16S Sequencing
Shallow Metagenomics
Metabolomics
B
d = 0.2
0.5mo
1mo
3mo
7mo
12mo
24mo
Parents
C
1 Phyla
Actinomycetota
Bacillota
Bacteroidota
Campylobacterota
Cyanobacteria
Desulfobacterota
Elusimicrobiota
Euryarchaeota
Fusobacteriota
Pseudomonadota
Verrucomicrobiota
Unknown
2 Time Point
0.5 months
1 month
3 months
7 months
12 months
24 months
Parents
3 Type of Birth
C-section
Vaginal
Parents
4 Feeding
Breast-fed
Formula-fed
Parents
D
Richness (zOTUs)
Sampling Time Point (months)
0.5
1
3
7
12
24
Parents
E
d = 0.2
F
Bifidobacteriales
Enterobacterales
Bacteroidales
Relative Abundance (%)
Cluster 1
Cluster 2
Cluster 3
****
G
Breastfeeding (exclusive)
Formula Amount (mean, ml)
Formula (any)
Number of Participants
Daily Formula Amount (ml)
Sampling Time Point (months)
H
Cluster 1
Cluster 2
Cluster 3
0.5mo
1mo
3mo
7mo
12mo
N=150
N=309
N=539
A
B
C
D
BF

604 **Figure 2 Temporal development of infant microbiota**
605 (A) Schematic of study fecal sample collection and time points of analysis of fecal samples.

606 (B) Non-metric multidimensional scaling (NMDS) plot of fecal samples grouped according to
607 infant age (months) or parent sample (separation of groups as whole is significant: $p \leq 0.001$,
608 permutational multivariate analysis based on distance matrices).

609 (C) *De novo* phylogenetic clustering of all study fecal samples (1222 fecal samples from 210
610 infants (multiple time points, including follow-up) and 152 parents (single time point))
611 displayed as a dendrogram, phyla per sample as stacked bar plots (second innermost ring),
612 metadata for each sample in the outermost three rings (feed type, type of birth and sampling
613 time point).

614 (D) Alpha-diversity (richness, zOTUs) at different infant sampling time points and for parental
615 samples. (**** = $p \leq 0.0001$, 25th to the 75th percentile box plot, median: solid line, whiskers:
616 min to max).

617 (E) Metric multidimensional scaling (MDS) plot of beta-diversity (unsupervised clustering) of
618 all infant samples (n= 998) producing three distinct clusters (separation of groups as whole is
619 significant: $p \leq 0.001$, permutational multivariate analysis based on distance matrices).

620 (F) Top 3 relative abundance (%) cluster dominating bacterial order violin plot (**** = $p \leq$
621 0.0001, median: solid line, 25th and 75th percentile: dashed lines), de novo generated clusters.

622 (G) Mean daily formula intake (ml, bar plot) and exclusive breastfeeding rates (grey line) versus
623 formula consumers (turquoise line).

624 (H) Descriptive cluster composition regarding sampling time point and feed type
625 (breastfeeding: grey, formula A (placebo): yellow, formula B (bifidobacteria): red, formula C
626 (GOS): green, formula D (bifidobacteria + GOS): dark blue).

627

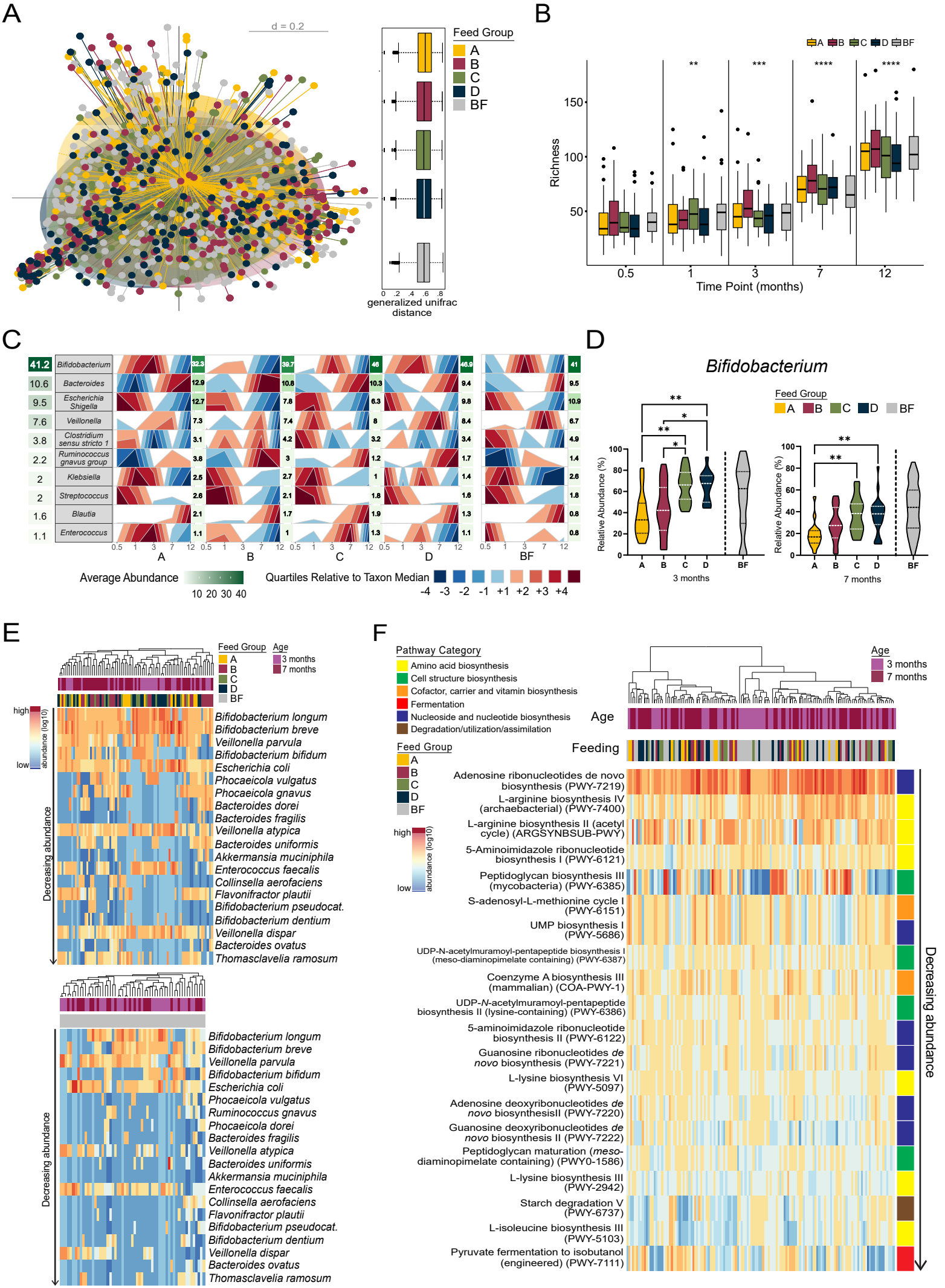
A
d = 0.2
Feed Group
A
B
C
D
BF
0 .2 .4 .6 .8
generalized unifrac distance
B
A B C D BF
Richness
150
100
50
0.5
1
3
7
12
Time Point (months)
C
Bifidobacterium
Bacteroides
Escherichia Shigella
Veillonella
Clostridium sensu stricto 1
Ruminococcus gnavus group
Klebsiella
Streptococcus
Blautia
Enterococcus
Average Abundance
10 20 30 40
Quartiles Relative to Taxon Median
-4 -3 -2 -1 +1 +2 +3 +4
D
Bifidobacterium
Feed Group
A B C D BF
Relative Abundance (%)
3 months
7 months
E
Feed Group
A
B
C
D
BF
Age
3 months
7 months
high
low
abundance (log10)
Decreasing abundance
Bifidobacterium longum
Bifidobacterium breve
Veillonella parvula
Bifidobacterium bifidum
Escherichia coli
Phocaeicola vulgatus
Phocaeicola gnavus
Bacteroides dorei
Bacteroides fragilis
Veillonella atypica
Bacteroides uniformis
Akkermansia muciniphila
Enterococcus faecalis
Collinsella aerofaciens
Flavonifractor plautii
Bifidobacterium pseudocat.
Bifidobacterium dentium
Veillonella dispar
Bacteroides ovatus
Thomasclavelia ramosum
F
Pathway Category
Amino acid biosynthesis
Cell structure biosynthesis
Cofactor, carrier and vitamin biosynthesis
Fermentation
Nucleoside and nucleotide biosynthesis
Degradation/utilization/assimilation
Feed Group
A
B
C
D
BF
Age
3 months
7 months
Feeding
Adenosine ribonucleotides de novo biosynthesis (PWY-7219)
L-arginine biosynthesis IV (archaebacterial) (PWY-7400)
L-arginine biosynthesis II (acetyl cycle) (ARGSYNBSUB-PWY)
5-Aminoimidazole ribonucleotide biosynthesis I (PWY-6121)
Peptidoglycan biosynthesis III (mycobacteria) (PWY-6385)
S-adenosyl-L-methionine cycle I (PWY-6151)
UMP biosynthesis I (PWY-5686)
UDP-N-acetylmuramoyl-pentapeptide biosynthesis I (meso-diaminopimelate containing) (PWY-6387)
Coenzyme A biosynthesis III (mammalian) (COA-PWY-1)
UDP-N-acetylmuramoyl-pentapeptide biosynthesis II (lysine-containing) (PWY-6386)
5-aminoimidazole ribonucleotide biosynthesis II (PWY-6122)
Guanosine ribonucleotides de novo biosynthesis (PWY-7221)
L-lysine biosynthesis VI (PWY-5097)
Adenosine deoxyribonucleotides de novo biosynthesisII (PWY-7220)
Guanosine deoxyribonucleotides de novo biosynthesis II (PWY-7222)
Peptidoglycan maturation (meso-diaminopimelate containing) (PWY0-1586)
L-lysine biosynthesis III (PWY-2942)
Starch degradation V (PWY-6737)
L-isoleucine biosynthesis III (PWY-5103)
Pyruvate fermentation to isobutanol (engineered) (PWY-7111)
Decreasing abundance

628 **Figure 3 Impact of bifidobacterial and GOS intervention on infant microbiota assembly**
629 (A) Infant beta-diversity (MDS plot) based on feed group. Boxplots show generalized UniFrac
630 distance for each of the five feed groups.

631 (B) Richness over time in the different feed groups (0.5:1 mo: ** = $p \leq 0.01$, 0.5:3 mo: *** =
632 $p \leq 0.001$, 0.5:7 mo and 0.5:12 mo **** = $p \leq 0.0001$, Anova $p < 2.2e{-}16$).

633 (C) Top 10 relative abundance (%) taxa (genus) found in >80% of samples (average abundance
634 >= 0.5). Color scale corresponding to increase (red) or decrease (blue) abundance relative to
635 the taxon median, average abundance per feed group in green boxes.

636 (D) Frequency distribution of the relative abundance of the genus *Bifidobacterium* (median:
637 solid line, upper and lower quartile: dotted line, ** = $p \leq 0.01$, * = $p \leq 0.05$). Minimal formula
638 consumers were omitted (lowest quartile based on daily formula volume consumption). Breast-
639 fed infants are figured on the right for comparison.

640 (E) Relative abundance (log values) of the top 20 species (shallow metagenomics) of individual
641 samples. Metadata as bars above samples (feeding, age) with hierarchal clustering at the very
642 top.

643 (F) Top 20 identified pathways (column normalized) associated with shallow metagenomic
644 sequencing samples sorted by decreasing abundance. Metadata as bars above samples (feeding,
645 age) with hierarchal clustering at the very top; pathway (BioCyc identifier), and pathway
646 categories on the left and right of the heatmap respectively.

647

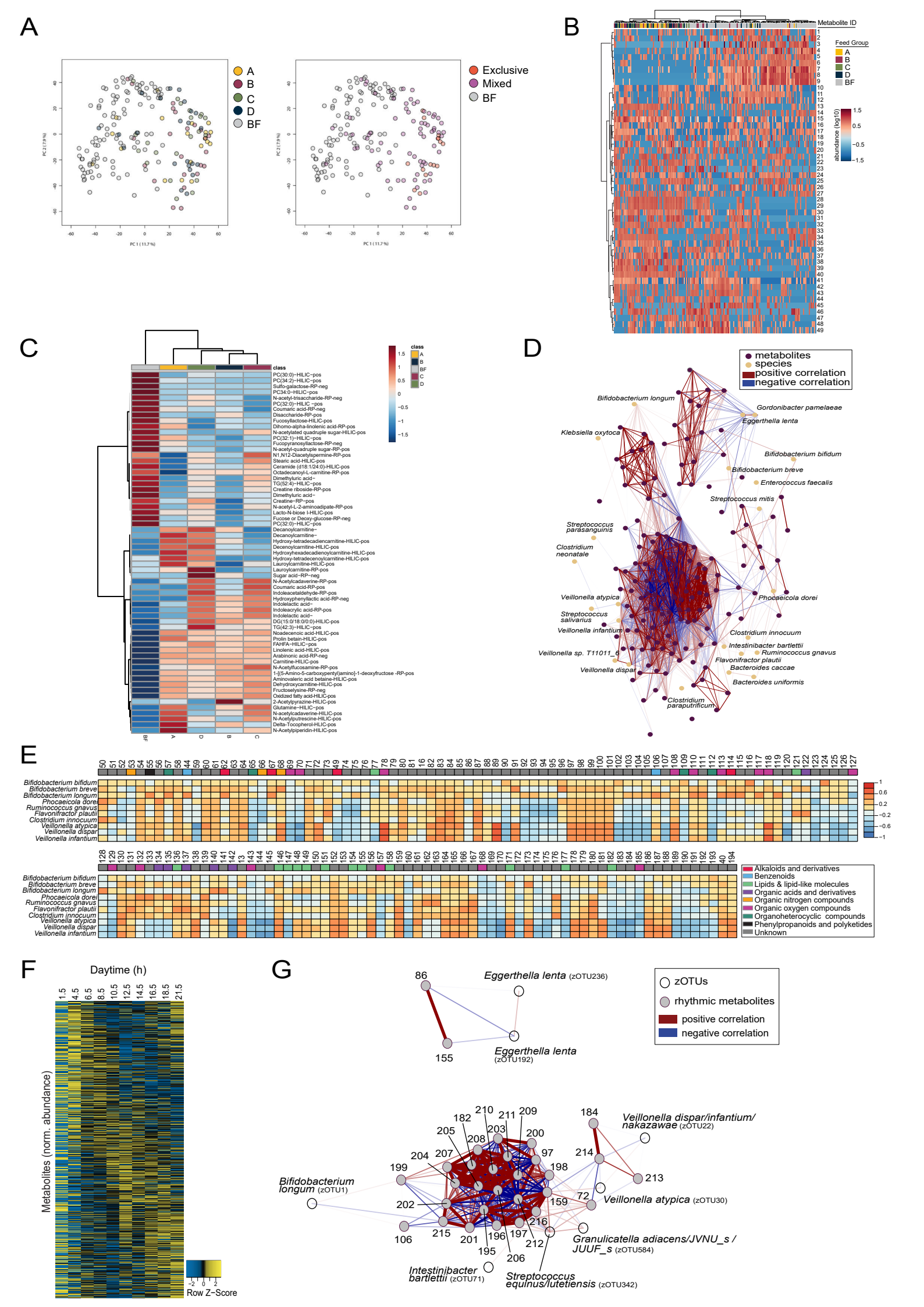
A
A
B
C
D
BF
Exclusive
Mixed
BF
PC 1 (11.7 %)
PC 2 (7.9 %)
B
Metabolite ID
Feed Group
A
B
C
D
BF
abundance (log10)
C
class
D
Bifidobacterium longum
Gordonibacter pamelaeae
Eggerthella lenta
Klebsiella oxytoca
Bifidobacterium bifidum
Bifidobacterium breve
Enterococcus faecalis
Streptococcus mitis
Streptococcus parasanguinis
Clostridium neonatale
Veillonella atypica
Phocaeicola dorei
Streptococcus salivarius
Veillonella infantium
Clostridium innocuum
Intestinibacter bartlettii
Ruminococcus gnavus
Flavonifractor plautii
Bacteroides caccae
Bacteroides uniformis
Clostridium paraputrificum
metabolites
species
positive correlation
negative correlation
E
Bifidobacterium bifidum
Bifidobacterium breve
Bifidobacterium longum
Phocaeicola dorei
Ruminococcus gnavus
Flavonifractor plautii
Clostridium innocuum
Veillonella atypica
Veillonella dispar
Veillonella infantium
Alkaloids and derivatives
Benzenoids
Lipids & lipid-like molecules
Organic acids and derivatives
Organic nitrogen compounds
Organic oxygen compounds
Organoheterocyclic compounds
Phenylpropanoids and polyketides
Unknown
F
Daytime (h)
Metabolites (norm. abundance)
Row Z-Score
G
Eggerthella lenta (zOTU236)
Eggerthella lenta (zOTU192)
zOTUs
rhythmic metabolites
positive correlation
negative correlation
Veillonella dispar/infantium/nakazawae (zOTU22)
Bifidobacterium longum (zOTU1)
Veillonella atypica (zOTU30)
Granulicatella adiacens/JVNU_s/JUUF_s (zOTU584)
Intestinibacter bartlettii (zOTU71)
Streptococcus equinus/lutetiensis (zOTU342)

648 **Figure 4 Metabolites clearly differentiate feeding groups and display circadian changes**
649 (A) Principal component analysis of infant metabolite profiles (3 months) stratified according
650 to feed type (left panel) and exclusive *vs* non-exclusive feeders (right panel).

651 (B) Intra-sample-normalized heatmap depicting the relative abundance of the top 49
652 metabolites found in infant fecal samples (3 months).

653 (C) Mean abundance of annotated fecal metabolites (3 months) displayed per feed group.

654 (D) Correlational network of fecal metabolites and species identified using shallow
655 metagenomics sequencing.

656 (E) Heatmap of significantly correlated ($r > 0.5$) species (shallow metagenomic sequencing)
657 and fecal metabolites, each metabolite is color-coded according to category affiliation to
658 MetaCyc pathways.

659 (F) Heatmap of normalized abundance of fecal metabolites at time-of-day intervals. Metabolites
660 are sorted by their peak abundance determined with a cosine-wave regression.

661 (G) Network correlational analysis of zOTUs and rhythmic metabolites. Thickness of
662 connecting lines indicates strength of correlation.

663

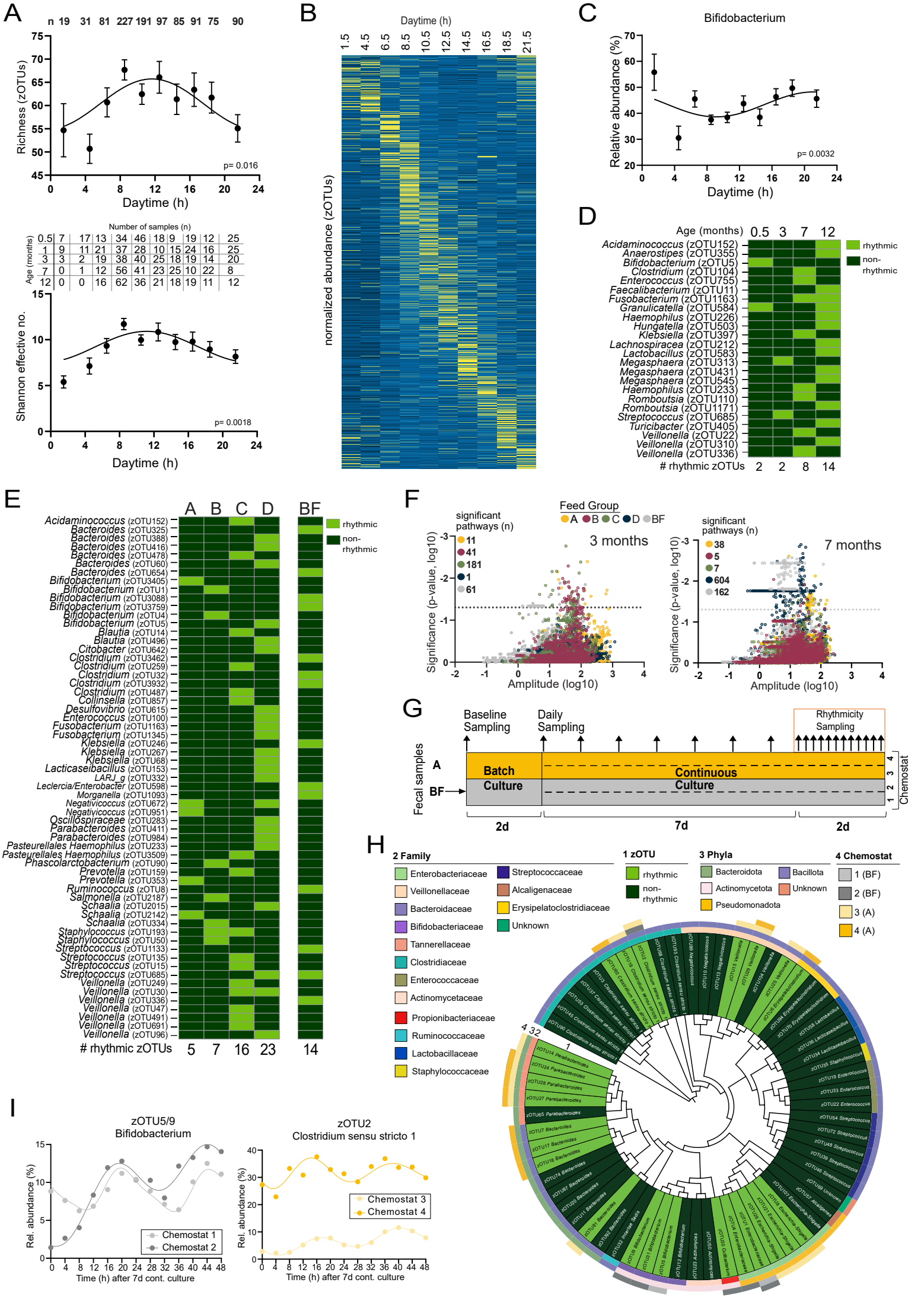
A
n 19 31 81 227 191 97 85 91 75 90
Richness (zOTUs)
p= 0.016
Daytime (h)
Number of samples (n)
Age (months)
Shannon effective no.
p= 0.0018
Daytime (h)
B
Daytime (h)
normalized abundance (zOTUs)
C
Bifidobacterium
Relative abundance (%)
p= 0.0032
Daytime (h)
D
Age (months) 0.5 3 7 12
rhythmic
non-rhythmic
rhythmic zOTUs 2 2 8 14
E
A B C D BF
rhythmic
non-rhythmic
rhythmic zOTUs 5 7 16 23 14
F
Feed Group
A B C D BF
significant pathways (n)
3 months
7 months
Significance (p-value, log10)
Amplitude (log10)
G
Baseline Sampling
Daily Sampling
Rhythmicity Sampling
Fecal samples
A
BF
Batch Culture
Continuous Culture
Chemostat
2d
7d
2d
H
2 Family
Enterobacteriaceae
Veillonellaceae
Bacteroidaceae
Bifidobacteriaceae
Tannerellaceae
Clostridiaceae
Enterococcaceae
Actinomycetaceae
Propionibacteriaceae
Ruminococcaceae
Lactobacillaceae
Staphylococcaceae
Streptococcaceae
Alcaligenaceae
Erysipelatoclostridiaceae
Unknown
1 zOTU
rhythmic
non-rhythmic
3 Phyla
Bacteroidota
Bacillota
Actinomycetota
Unknown
Pseudomonadota
4 Chemostat
1 (BF)
2 (BF)
3 (A)
4 (A)
I
zOTU5/9
Bifidobacterium
Rel. abundance (%)
Chemostat 1
Chemostat 2
Time (h) after 7d cont. culture
zOTU2
Clostridium sensu stricto 1
Rel. abundance (%)
Chemostat 3
Chemostat 4
Time (h) after 7d cont. culture

664 **Figure 5 Developing daytime-related rhythmicity of the infant microbiota is affected by**
665 **formula supplementation**
666 (A) Diurnal profiles of alpha-diversity of samples with known time of defecation (n = 987),
667 displayed as mean ± SEM. Number of total samples at each time point are shown above the
668 graph, number of samples per time of day per age group are displayed in the table in graph.

669 (B) Heatmap of relative abundance of 777 zOTUs detected in infant samples (mean relative
670 abundance > 1%, normalized to peak per zOTU) ordered by time of cosine-wave amplitude
671 peak of the zOTUs.

672 (C) Diurnal profile of the genus *Bifidobacterium* across all infant samples.

673 (D) Rhythmic zOTUs at age 0.5, 3, 7 and 12 months with the total number of rhythmic zOTUs
674 displayed at the bottom of the graph.

675 (E) Rhythmic zOTUs in the five feeding groups with the total number of rhythmic zOTUs
676 displayed at the bottom of the graph.

677 (F) Quantification and significance of rhythmic and arrhythmic pathways in infant samples (3
678 and 7 months), separated by feed group. Significantly rhythmic pathways are located above the
679 dashed line ($p < 0.05$).

680 (G) Schematic illustration of study design and sampling time points of chemostats 1-4
681 containing stool cultures obtained from breastfed (BF) and placebo formula (A) fed infants.

682 (H) Phylogenetic clustering of zOTUs identified in chemostat samples, displayed as a
683 cladogram. Rhythmicity is indicated for the individuals zOTUS (ring 1), family (ring 2), phyla
684 (ring 3) and in which chemostat the rhythmic zOTUs were found (ring 4).

685 (I) Circadian profiles of zOTUs from chemostat cultures after 7 days of continuous culture.
686 Significant rhythms are illustrated with fitted cosine-wave curves (cosine-wave regression, $p \leq$
687 0.05). Data are represented as mean ± SEM.

Tables

Table 1 Cohort characteristics of enrolled infants

Values are given in median with interquartile range in parenthesis unless otherwise indicated.

	A		B		C		D		BF	
N	35	-	39	-	36	-	37	-	63	-
Samples (n)	119	-	136	-	125	-	135	-	483	-
Discontinue study (N)	4	-	2	-	1	-	2	-	2	-
Birth characteristics										
Gestational age (days)	279.0	(272.0-284.0)	277.0	(271.0-284.0)	279.5	(273.5-284.0)	278.0	(273.0-282.5)	278.0	(270.0-285.0)
Weight (g)	3450	(3100-3725)	3250	(2960-3640)	3410	(2903-3893)	3370	(3060-3585)	3360	(3015-3690)
Size (cm)	52.0	(50.0-53.0)	51.0	(49.0-53.0)	51.5	(50.0-53.0)	51.0	(50.0-52.5)	52.0	(50.0-53.0)
Cesaerean delivery, %	37.1	-	25.6	-	38.9	-	40.5	-	27.0	-
Female, %	51.4	-	61.5	-	30.6	-	58.3	-	50.8	-
Male, %	48.6	-	38.5	-	69.4	-	43.2	-	49.2	-
Twin, %	0	-	10.3	-	11.1	-	10.8	-	6.3	-
Maternal characteristics										
BMI pre pregnancy, kg/m2, mean	23.2		22.7		22.7		23.9		22.0	
Age at inclusion (years), mean	34.2		33.1		33.3		32.7		33.4	
Nuclear family characteristics										
Atopic disease, %	57.1	-	59.0	-	50.0	-	51.4	-	60.3	-
Autoimmune disease, %	8.6	-	2.6	-	5.6	-	8.1	-	11.1	-
Environment										
Animal contact, %	31.4	-	38.5	-	27.8	-	35.1	-	30.2	-
Distance to study center (km),mean	36.60		36.2		41.20		39.9		41.7	
Siblings in household, %	22.9	-	30.8	-	25	-	37.8	-	44.4	-
Sample characteristics										
Breastfeeding during first year, % (N)	88.6	-	87.2	-	91.7	-	83.8	-	100	-
Exclusive formula-feeding, % (N)	11.4	-	12.8	-	8.3	-	16.2	-	0	-
Daily formula intake (ml)	480.0	(200.0-720.0)	500	(242.5-700.0)	400.0	(220.0-750.0)	505	(217.5-657.5)	0	0
Age start solid food (months)	4.9	(4.4-5.8)	4.9	(4.2-5.4)	5	(4.6-5.8)	4.6	(4.0-6.1)	5.5	(5.0-6.1)

Supplemental Figure 1

A

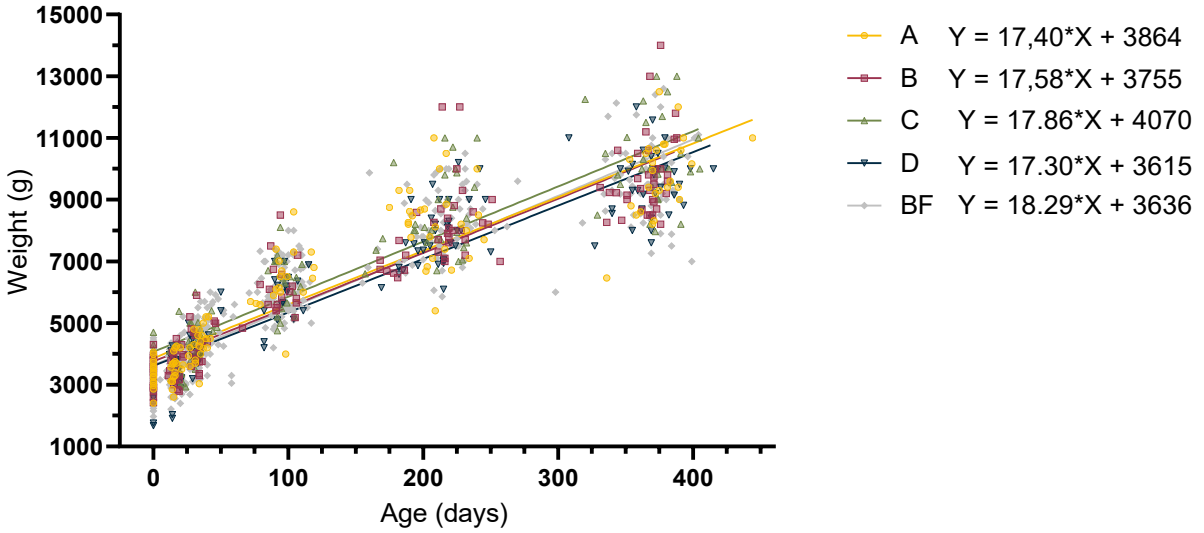

B

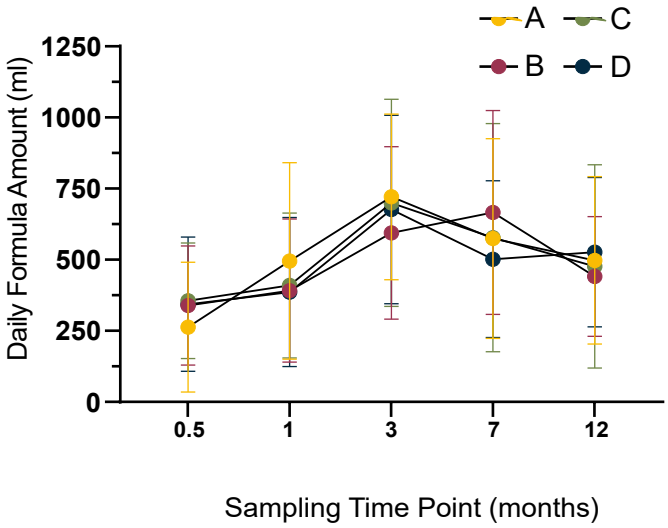

C

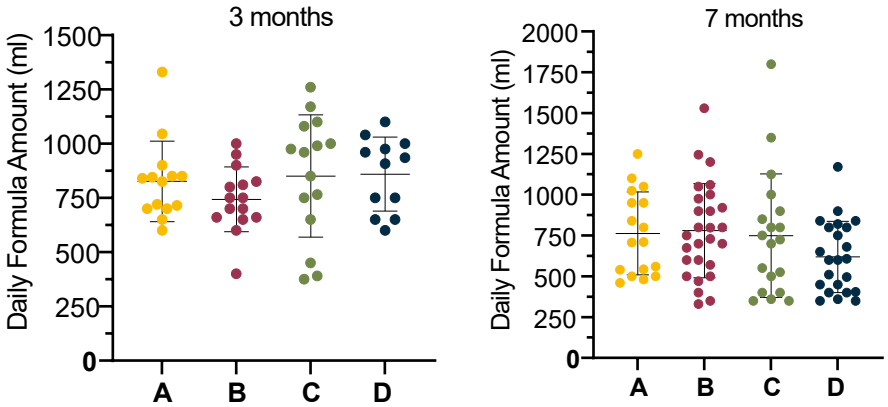

D

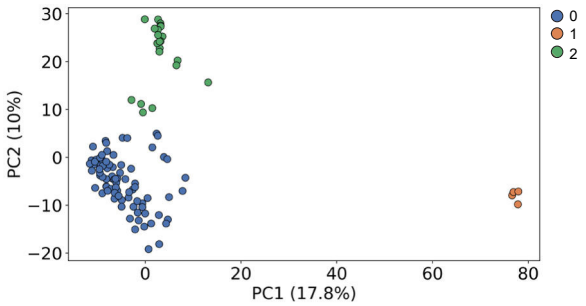

E

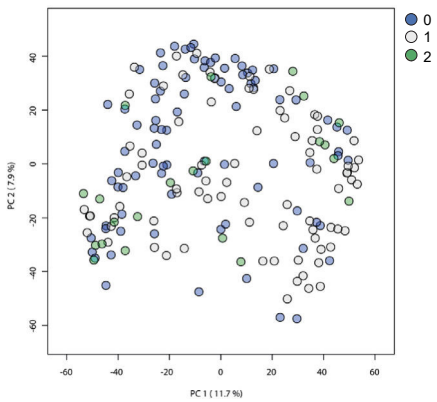

692 **Supplemental Figure 1: Intervention groups and breastfeeders are comparable with**
693 **regards to weight gain and formula consumption**
694 (A) Longitudinal weight gain of study participants in the different feeding groups (linear
695 regression, slopes are not significantly different).

696 (B) Daily amount of formula (ml) consumed (mean with SD) per interventional group at
697 different sampling time points.

698 (C) Formula amount consumption (ml) of infants where minimal formula consumers were
699 omitted (lowest quartile based on daily formula volume consumption) at age 3 and 7 months
700 (mean, SD).

701 (D) Principal component analysis of 103 breastmilk samples (1-month), with unsupervised
702 clustering (k-means) by color. t-Test (clusters 0 and 2): 306 significant metabolites on 1439
703 total (p-value threshold 0.05).

704 (E) Principal component analysis of infant metabolite profiles (3-months) in feces, with
705 breastmilk clusters differentiated by color. t-Test showed no significance between clusters
706 among 4895 metabolites (p-value threshold 0.05).

Supplemental Figure 2

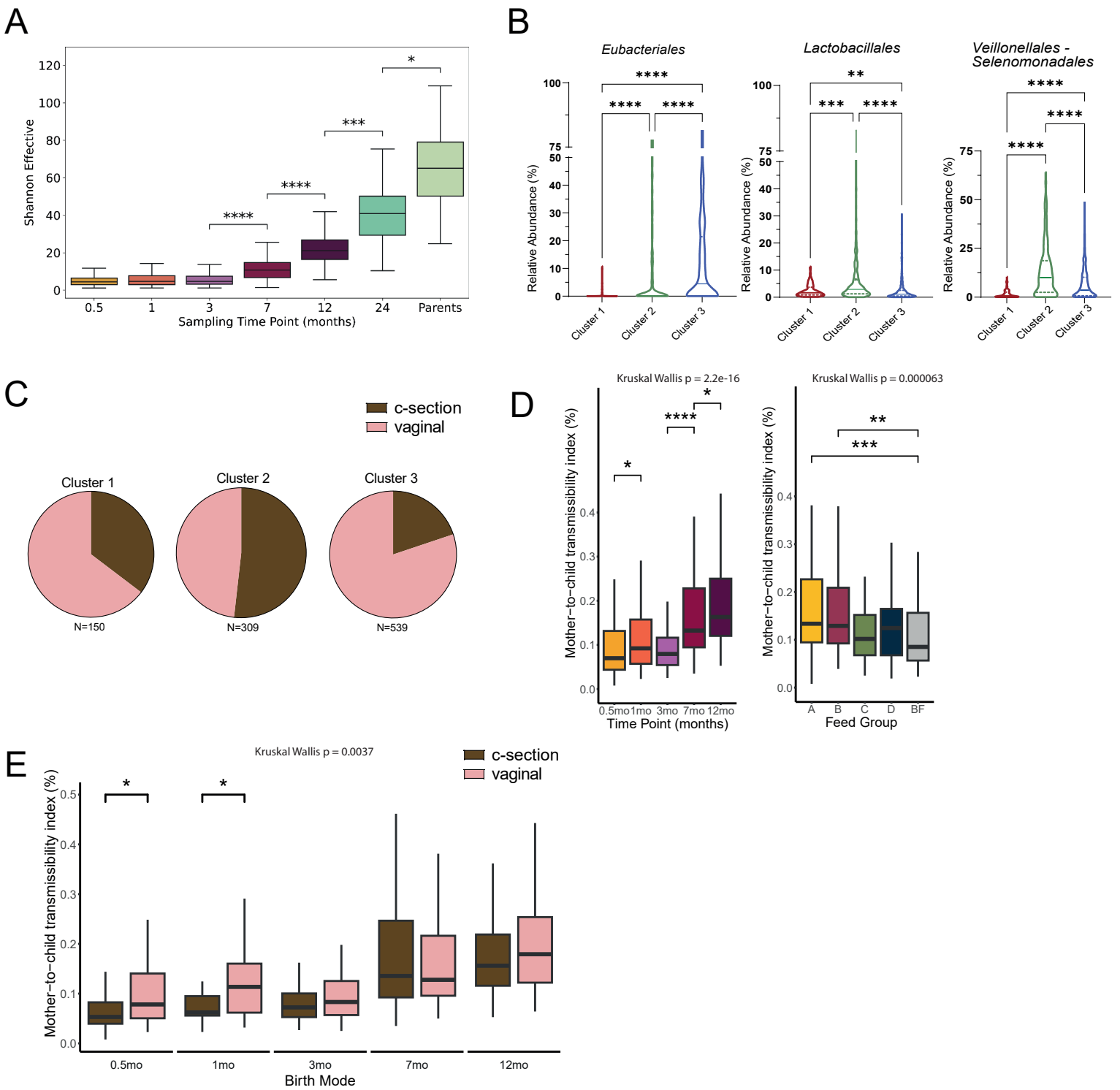

Supplemental Figure 2: Changes of infant fecal microbiota in relation to age, birth mode and feeding type

(A) Alpha-diversity (Shannon effective number) at all infant sampling time points (including 24 months) and for parental samples (**** = $p \leq 0.0001$, 25th to the 75th percentile box plot, median: solid line, whiskers: min to max).

(B) Top 4-6 relative abundance (%) cluster dominating bacterial order violin plot (**** = $p \leq 0.0001$, median: solid line, 25th and 75th percentile: dashed lines), de novo generated clusters.

(C) Birth mode (C-section vs. vaginal) distribution in the three clusters.

(D, E) Bacterial (zOTUs) transmissibility ratio (%) between mother and infant over time during the 1st year of life (D, left panel) and according to the feed group (D, right panel) or according to sampling time and birth mode (E). (Dunn test: * = $p<0.05$, ** = $p<0.01$, *** = $p<0.001$, **** = $p<0.0001$)).

Supplemental Figure 3

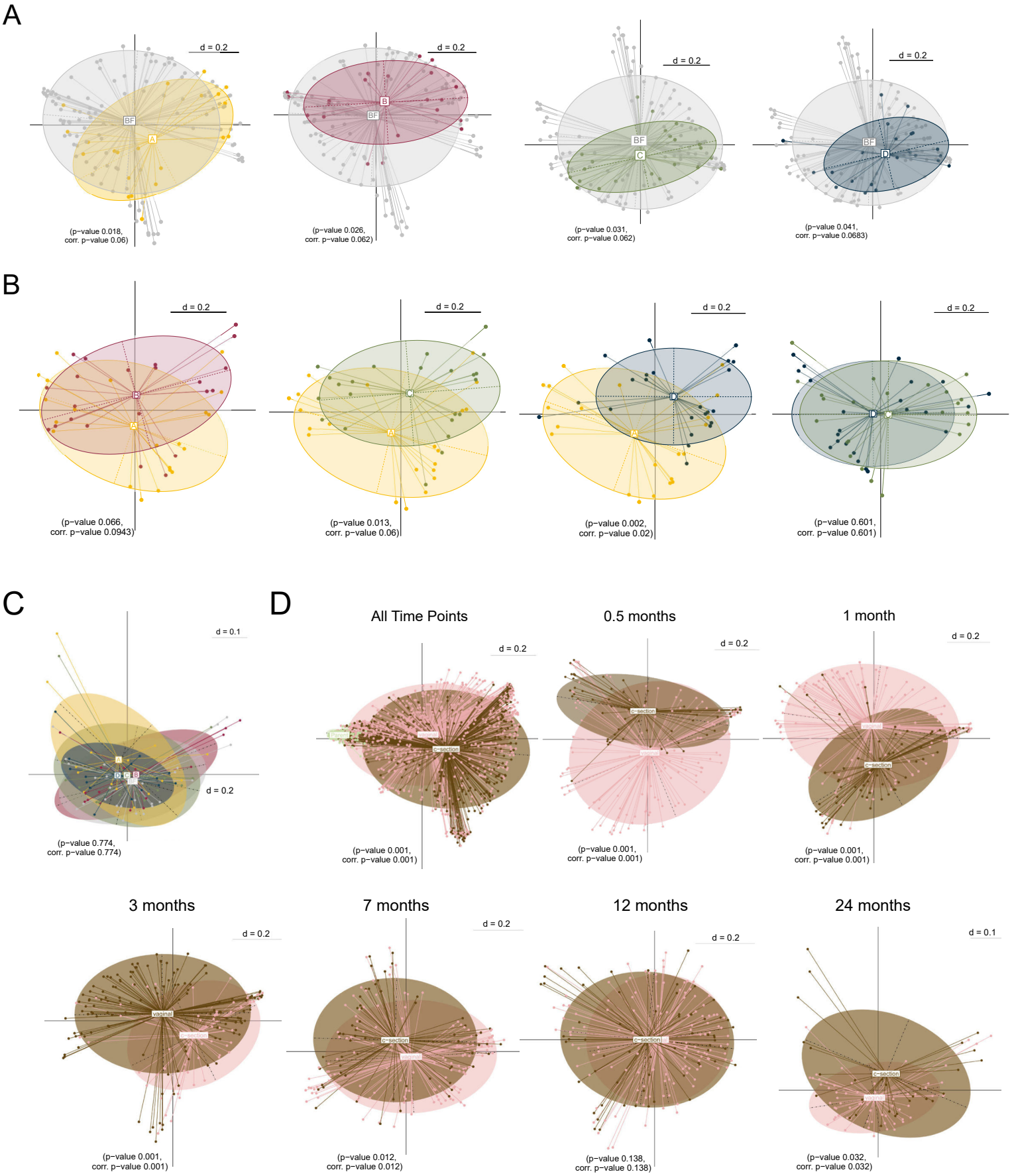

719 **Supplemental Figure 3: Bacterial profiling in response to feeding and birth mode**
720 (A) MDS plots of beta-diversity comparison between breastfeeders and formula groups at 3
721 months.

722 (B) MDS plots of beta-diversity comparison between placebo formula A and other groups at 3
723 months and between C and D.

724 (C) MDS plot of beta-diversity comparison between all feed groups at 24-months.

725 (D) MDS plots of beta-diversity comparisons between vaginal and C-section birth modes
726 overall in the 1st year of life and at each time point.

Supplemental Figure 4

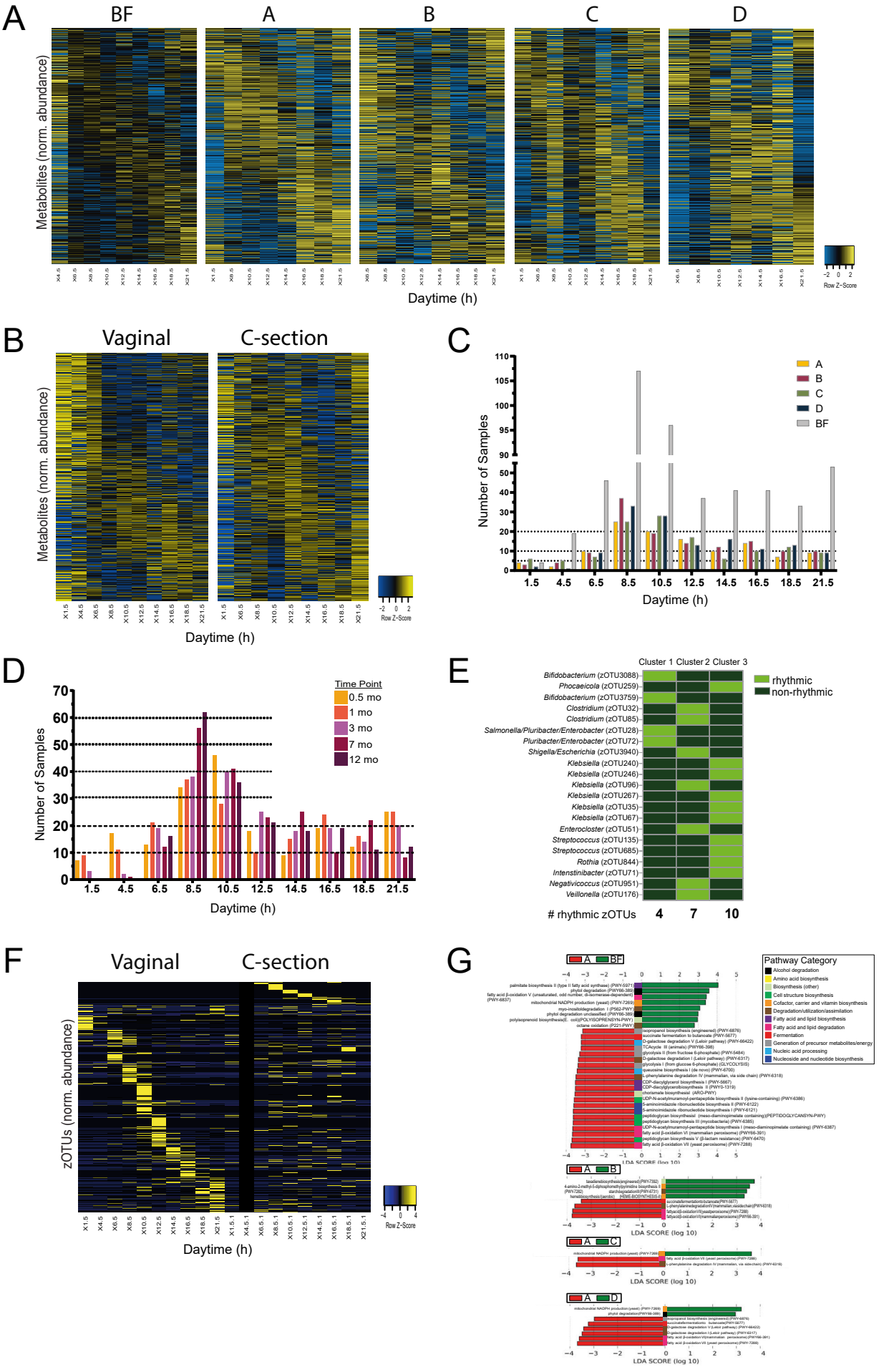

Supplemental Figure 4: Differences in daytime sampling and rhythmicity in unsupervised clusters and between feed groups and birth mode

(A, B) Heatmaps of normalized abundance of fecal metabolites at time-of-day intervals for each feeding group (A) (1822 metabolites) and birth mode (B) (2317 metabolites). Metabolites were sorted by their peak abundance determined with a cosine-wave regression in each of the groups.

(C) Number of fecal samples at different times of day (hours) per feed group.

(D) Number of fecal samples at different times of day (hours) per sampling time point.

(E) Rhythmic zOTUs in the three de novo clusters with the total number of rhythmic zOTUs displayed at the bottom of the graph.

(F) Heatmap of normalized abundance of 948 zOTUs at time-of-day intervals by birth mode. zOTUs were sorted by their peak abundance determined with a cosine-wave regression in the C-section and then the vaginal group.

(G) Linear discriminant analysis (LDA) effect size (LEfSe) of pathways at age 7 months between placebo formula group (A) and all other feeding groups (formula B, C, D and breastfeeding (BF)).

Supplemental Figure 5

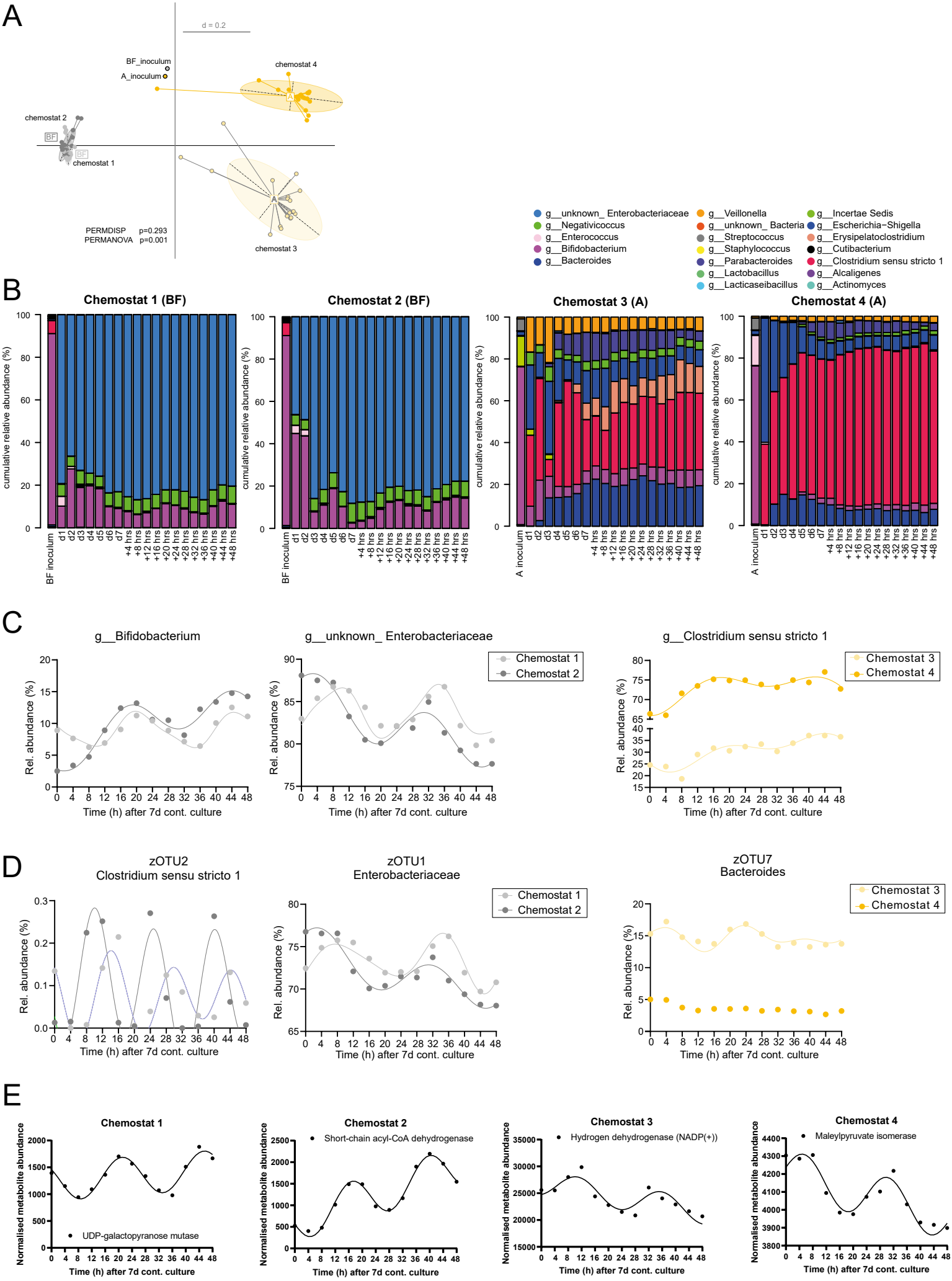

742 **Supplemental Figure 5: Chemostats differ in taxonomic composition and diversity but**
743 **consistently show rhythmicity in all vessels**
744 (A) MDS plot of beta-diversity comparison between placebo formula A and BF of the *ex vivo*
745 chemostat samples and the inoculum samples (separation of groups as whole is significant: $p \leq$
746 0.001, permutational multivariate analysis based on distance matrices). BF_chemostat_1-
747 BF_chemostat_2: corr. p-value 0.0627, BF_chemostat_1-A_chemostat_3: corr. p-value 0.003,
748 BF_chemostat_1-A_chemostat_4: corr. p-value 0.003, BF_chemostat_2-A_chemostat_3: corr.
749 p-value 0.003, BF_chemostat_2-A_chemostat_4: corr. p-value 0.003, A_chemostat_3-
750 A_chemostat_4: corr. p-value 0.003

751 (B) Taxonomic binning barplots showing the differences in taxonomic composition of each
752 chemostat throughout the continuous culture and rhythmicity sampling period.

753 (C-E) Circadian profiles of genera (C), zOTUs (D) and metabolic pathways (PICRUSt2) (E)
754 from chemostat cultures after 7 days of continuous culture. Significant rhythms are illustrated
755 with fitted cosine-wave curves (cosine-wave regression, $p \leq 0.05$). For zOTU7, chemostat 4 is
756 not significantly rhythmic. Data are represented as mean ± SEM.

757 **Supplemental Table 1: untargeted metabolomics**

Nr in Figure	Fig	Original ID	RT [sec]	m/z	Compound Name
1	4C/4D	ID1878_RP_pos	445.2965	584.2579	unknown
2	4C/4D	ID2147_HILIC_pos	41.3172	872.7654	TG(52:4)
3	4C/4D	ID823_RP_neg	47.9137	855.3091	unknown
4	4C/4D	ID1240_RP_pos	45.7357	381.0789	Disaccharide
5	4C/4D	ID1843_HILIC_pos	46.7741	732.5525	PC(32:1)
6	4C/4D	ID1295_HILIC_pos	325.4208	527.3134	unknown
7	4C/4D	ID1979_RP_pos	47.5239	708.2544	N-acetyl-quadruple sugar
8	4C/4D	ID2155_HILIC_pos	530.2239	878.2997	unknown
9	4C/4D	ID2205_HILIC_pos	569.4872	1387.4841	unknown
10	4C/4D	ID666_HILIC_pos	265.5851	337.2509	unknown
11	4C/4D	ID666_RP_neg	520.0732	539.2167	unknown
12	4C/4D	ID784_RP_neg	519.3508	805.5629	unknown
13	4C/4D/4F	ID338_HILIC_pos	45.5292	213.1824	unknown
14	4C/4D	ID947_RP_pos	645.0067	325.2108	unknown
15	4C/4D	ID554_HILIC_pos	41.3418	297.2767	Noadecenoic acid
16	4C/4D/4F	ID1067_RP_pos	449.214	345.2824	unknown
17	4C/4D	ID194_RP_neg	632.1141	295.189	unknown
18	4C/4D	ID1495_HILIC_pos	466.705	604.2497	unknown
19	4C/4D	ID1524_RP_pos	671.0764	430.3485	unknown
20	4C/4D	ID1462_HILIC_pos	345.6149	591.3413	unknown
21	4C/4D	ID203_HILIC_pos	44.6892	165.0937	unknown
22	4C/4D	ID951_HILIC_pos	43.9798	424.3549	unknown
23	4C/4D	ID1501_HILIC_pos	276.4828	604.5999	unknown
24	4C/4D	ID1075_RP_pos	361.9261	351.1558	unknown
25	4C/4D	ID1989_RP_pos	708.0827	763.6034	unknown
26	4C/4D	ID276_RP_neg	544.2773	375.33	unknown
27	4C/4D	ID1872_HILIC_pos	45.5417	747.5897	unknown
28	4C/4D	ID279_RP_pos	587.4899	182.161	unknown
29	4C/4D	ID528_RP_pos	587.51	249.2476	unknown
30	4C/4D	ID1448_HILIC_pos	44.9654	583.5245	DG(15:0/18:0/0:0)
31	4C/4D	ID932_RP_pos	560.2321	322.2425	unknown
32	4C/4D	ID328_HILIC_pos	45.7918	209.187	unknown
33	4C/4D	ID425_HILIC_pos	70.027	255.0003	unknown
34	4C/4D	ID52_RP_pos	882.4914	97.9682	unknown
35	4C/4D	ID1543_RP_pos	298.375	433.2828	unknown
36	4C/4D	ID579_RP_neg	36.9573	502.914	unknown
37	4C/4D	ID957_HILIC_pos	44.3644	425.3386	Delta-Tocopherol
38	4C/4D	ID131_HILIC_pos	409.5396	144.0998	Prolin betain
39	4C/4D	ID962_HILIC_pos	78.185	426.1919	unknown
40	4C/4D/4F	ID2104_HILIC_pos	44.2302	832.669	unknown
41	4C/4D	ID1884_HILIC_pos	107.927	755.6154	TG(42:3)
42	4C/4D	ID1586_HILIC_pos	130.8504	635.6108	unknown
43	4C/4D	ID2017_HILIC_pos	129.2633	801.6593	unknown

44	4C/4D/4F	ID205_RP_pos	276.8442	165.0539	Coumaric acid
45	4C/4D	ID668_RP_pos	254.763	280.1055	unknown
46	4C/4D	ID1138_HILIC_pos	396.2653	472.1415	unknown
47	4C/4D	ID519_RP_neg	439.0721	474.2547	unknown
48	4C/4D	ID136_RP_pos	68.6502	145.1328	N-Acetylcadaverine
49	4C/4D/4F	ID719_RP_pos	47.173	287.241	N1,N12-Diacetylspermine
50	4F	ID13_RP_pos	45.6086	58.0649	unknown
51	4F	ID32_RP_pos	48.5084	72.0808	unknown
52	4F	ID61_RP_pos	43.7121	104.1066	unknown
53	4F	ID98_RP_pos	47.0312	132.0761	Creatine
54	4F	ID125_RP_pos	587.6851	143.1058	unknown
55	4F	ID143_RP_pos	276.9252	147.0429	Coumarin (low hit rate 48.72%)
56	4F	ID170_RP_pos	587.6044	155.178	unknown
57	4F	ID184_RP_pos	337.5045	160.0748	Indoleacetaldehyde
58	4F	ID200_RP_pos	587.5189	164.1504	unknown
59	4F	ID250_RP_pos	507.8812	174.1303	unknown
60	4F	ID262_RP_pos	587.4744	178.1659	unknown
61	4F	ID300_RP_pos	587.5718	186.1558	unknown
62	4F	ID305_RP_pos	337.5045	188.07	Indoleacrylic acid
63	4F	ID318_RP_pos	587.5566	192.1818	unknown
64	4F	ID336_RP_pos	587.5244	196.1768	unknown
65	4F	ID340_RP_pos	268.5427	197.0664	Dimethyluric acid
66	4F	ID365_RP_pos	47.7627	204.0862	N-acetyl-L-2-aminoadipate
67	4F	ID375_RP_pos	338.6819	206.0805	Indolelactic acid
68	4F	ID377_RP_pos	43.3248	206.1021	N-Acetylfucosamine
69	4F	ID515_RP_pos	47.3348	247.0927	unknown
70	4F	ID586_RP_pos	47.2125	264.1182	Creatine riboside
71	4F	ID591_RP_pos	591.3177	265.2523	unknown
72	4F/4H	ID637_RP_pos	43.2368	273.1433	unknown
73	4F	ID699_RP_pos	38.3207	284.9259	unknown
74	4F	ID782_RP_pos	709.7177	299.1386	unknown
75	4F	ID797_RP_pos	709.6879	300.1412	unknown
76	4F	ID814_RP_pos	374.105	302.2304	unknown
77	4F	ID843_RP_pos	655.1938	307.2623	Dihomo-alpha-linolenic acid
78	4F	ID853_RP_pos	43.1228	309.1652	1-[(5-Amino-5-carboxypentyl)amino] -1-deoxyfructose
79	4F	ID899_RP_pos	408.5222	316.2476	Decanoylcarnitine
80	4F	ID918_RP_pos	587.8349	318.2994	unknown
81	4F	ID1062_RP_pos	449.149	344.2793	Lauroylcarnitine
82	4B/4F	ID1148_RP_pos	269.0495	367.1495	unknown
83	4B/4F	ID1182_RP_pos	279.9274	371.2175	unknown
84	4F	ID1195_RP_pos	279.7921	372.2206	unknown
85	4F	ID1249_RP_pos	47.249	383.1374	unknown
86	4F/4H	ID1276_RP_pos	424.3017	386.2411	unknown
87	4F	ID1299_RP_pos	279.4737	389.2283	unknown

88	4F	ID1385_RP_pos	385.0854	402.283	unknown
89	4F	ID1706_RP_pos	44.7933	471.2175	unknown
90	4F	ID1843_RP_pos	437.6435	552.3348	unknown
91	4F	ID1858_RP_pos	275.0814	569.2906	unknown
92	4F	ID1867_RP_pos	445.3817	583.2545	unknown
93	4F	ID1882_RP_pos	709.7493	585.2672	unknown
94	4F	ID1907_RP_pos	709.232	604.2229	unknown
95	4F	ID1914_RP_pos	709.8671	607.2511	unknown
96	4F	ID1923_RP_pos	548.5101	617.3865	unknown
97	4F/4H	ID1932_RP_pos	587.3156	639.485	unknown
98	4F	ID1948_RP_pos	587.6053	657.459	unknown
99	4F	ID1953_RP_pos	587.5339	658.462	unknown
100	4F	ID1955_RP_pos	587.5718	659.4563	unknown
101	4F	ID1959_RP_pos	587.5208	660.4575	unknown
102	4F	ID4_RP_neg	44.3665	88.0397	unknown
103	4F	ID54_RP_neg	45.4521	162.0766	unknown
104	4F	ID56_RP_neg	49.2802	163.0616	Fucose or Deoxy-glucose
105	4F	ID57_RP_neg	71.257	163.0615	unknown
106	4F/4H	ID58_RP_neg	280.2972	163.0388	Coumaric acid
107	4F	ID62_RP_neg	49.3001	164.0641	unknown
108	4F	ID67_RP_neg	47.5997	165.0402	Arabinonic acid (98.25%)
109	4F	ID72_RP_neg	88.6861	167.021	unknown
110	4F	ID82_RP_neg	280.4396	181.0507	Hydroxyphenyllactic acid
111	4F	ID85_RP_neg	280.1192	182.0535	unknown
112	4F	ID97_RP_neg	271.8839	195.0522	Dimethyluric acid
113	4F	ID98_RP_neg	47.1844	195.0506	Sugar acid
114	4F	ID104_RP_neg	346.4323	204.0671	Indolelactic acid
115	4F	ID107_RP_neg	346.0053	205.0695	unknown
116	4F	ID136_RP_neg	53.2571	259.0136	3-O-sulfo-β-D-galactose
117	4F	ID147_RP_neg	347.5474	272.054	unknown
118	4F	ID215_RP_neg	44.3295	307.1504	Fructoselysine
119	4F	ID269_RP_neg	570.8473	365.2306	unknown
120	4F	ID280_RP_neg	46.2214	380.1617	unknown
121	4F	ID297_RP_neg	492.7667	389.2698	unknown
122	4F	ID398_RP_neg	492.7135	435.2752	unknown
123	4F	ID416_RP_neg	39.8382	440.8856	unknown
124	4F	ID481_RP_neg	58.5597	462.0931	unknown
125	4F	ID573_RP_neg	418.5118	499.3269	unknown
126	4F	ID599_RP_neg	429.2894	513.3428	unknown
127	4F	ID630_RP_neg	53.4444	523.1444	fucopyranosyllactose
128	4F	ID656_RP_neg	420.7276	536.3211	unknown
129	4F	ID677_RP_neg	47.9845	546.2038	N-acetyl-trisaccharide
130	4B/4F	ID788_RP_neg	282.616	811.4574	unknown
131	4F	ID8_HILIC_pos	424.4444	60.0803	unknown
132	4F	ID80_HILIC_pos	385.1537	123.0541	2-Acetylpyrazine
133	4F	ID85_HILIC_pos	351.9125	128.1056	N-Acetylpiperidin

134	4F	ID97_HILIC_pos	369.6011	131.1162	N-Acetylputrescine
135	4F	ID137_HILIC_pos	352.4391	145.1325	N-acetylcadaverine
136	4F	ID141_HILIC_pos 100%	424.348	146.1171	3-Dehydroxycarnitine
137	4F	ID145_HILIC_pos	424.3643	147.1195	Glutamine
138	4F	ID161_HILIC_pos	97.413	153.0638	unknown
139	4F	ID170_HILIC_pos	332.2044	159.1481	unknown
140	4F	ID189_HILIC_pos	405.4134	162.1117	Carnitine
141	4F	ID193_HILIC_pos	405.2537	163.1126	unknown
142	4F	ID245_HILIC_pos	312.4109	175.0703	unknown
143	4F	ID449_HILIC_pos	439.5683	264.1192	unknown
144	4F	ID454_HILIC_pos	439.7345	265.1215	unknown
145	4F	ID518_HILIC_pos	357.7949	284.062	unknown
146	4B/4F	ID550_HILIC_pos	45.7972	295.2258	oxidized fatty acid
147	4F	ID582_HILIC_pos	44.1117	307.261	stearic acid
148	4F	ID607_HILIC_pos	291.0532	314.231	Decenoylcarnitine
149	4F	ID614_HILIC_pos	289.283	316.247	Decanoylcarnitine
150	4F	ID680_HILIC_pos	284.8135	342.2629	unknown
151	4F	ID688_HILIC_pos	283.692	344.2791	Lauroylcarnitine
152	4B/4F	ID768_HILIC_pos	307.4853	371.218	unknown
153	4F	ID784_HILIC_pos	459.039	381.1279	unknown
154	4F	ID795_HILIC_pos	292.5264	384.2727	Hydroxy-tetradecadiencarnitine
155	4F/4H	ID807_HILIC_pos	289.7417	386.2895	Hydroxy-tetradecenoylcarnitine
156	4F	ID839_HILIC_pos	50.7572	397.378	unknown
157	4F	ID876_HILIC_pos	416.8625	406.1316	Lacto-N-biose I
158	4F	ID899_HILIC_pos	287.1428	412.3056	Hydroxyhexadecadienoylcarnitine
159	4F/4H	ID948_HILIC_pos	43.7895	423.3233	unknown
160	4F	ID983_HILIC_pos	274.8781	429.3742	unknown
161	4F	ID1001_HILIC_pos	43.2323	431.3727	unknown
162	4F	ID1015_HILIC_pos	395.6925	434.1883	unknown
163	4F	ID1021_HILIC_pos	395.6508	435.1907	unknown
164	4F	ID1062_HILIC_pos	42.4714	446.397	unknown
165	4F	ID1071_HILIC_pos	42.6837	447.4	unknown
166	4F	ID1074_HILIC_pos	42.8372	448.3988	unknown
167	4F	ID1105_HILIC_pos	52.8675	459.3401	unknown
168	4F	ID1231_HILIC_pos	461.7946	511.1628	3-Fucosyllactose
169	4F	ID1345_HILIC_pos	43.8975	548.5346	unknown
170	4F	ID1346_HILIC_pos	97.4613	548.5369	unknown
171	4F	ID1380_HILIC_pos	44.23	561.4887	FAHFA
172	4F	ID1399_HILIC_pos	80.4379	567.4422	unknown
173	4F	ID1425_HILIC_pos	46.2204	573.4763	unknown
174	4F	ID1431_HILIC_pos	43.6126	576.566	unknown
175	4F	ID1565_HILIC_pos	92.2118	630.6151	unknown
176	4F	ID1604_HILIC_pos	227.4001	642.5123	unknown
177	4F	ID1621_HILIC_pos	44.7479	650.6385	Ceramide (d18:1/24:0)
178	4F	ID1661_HILIC_pos	40.811	663.4519	unknown

179	4F	ID1663_HILIC_pos	41.092	664.4597	unknown
180	4F	ID1707_HILIC_pos	45.8138	678.5186	unknown
181	4F	ID1726_HILIC_pos	512.4292	689.2044	unknown
182	4F/4H	ID1780_HILIC_pos	256.9355	706.5366	PC(30:0)
183	4F	ID1790_HILIC_pos	98.0462	710.5901	unknown
184	4F/4H	ID1792_HILIC_pos	97.5934	711.5925	unknown
185	4F	ID1794_HILIC_pos	494.3389	714.242	N-acetylated quadruple sugar
186	4F	ID1812_HILIC_pos	46.2407	719.57	unknown
187	4F	ID1822_HILIC_pos	46.1982	721.5722	unknown
188	4F	ID1876_HILIC_pos	44.335	749.601	unknown
189	4F	ID1989_HILIC_pos	84.2318	792.6685	unknown
190	4F	ID1992_HILIC_pos	86.5068	793.6716	unknown
191	4F	ID1994_HILIC_pos	92.0972	794.6834	unknown
192	4F	ID1998_HILIC_pos	76.3574	795.6861	unknown
193	4F	ID2074_HILIC_pos	200.7976	819.6667	unknown
194	4F	ID2163_HILIC_pos	42.3567	880.7645	unknown
195	4B/4H	ID990_HILIC_pos	42.9535	430.3752	unknown
196	4H	ID989_HILIC_pos	43.0046	429.3716	unknown
197	4H	ID971_HILIC_pos	43.8123	427.3523	unknown
198	4H	ID924_RP_pos	40.5003	320.8688	unknown
199	4H	ID580_RP_pos	560.4512	263.2366	unknown
200	4H	ID503_HILIC_pos	46.0612	279.2291	Linolenic acid
201	4H	ID2187_HILIC_pos	548.1752	1022.3515	unknown
202	4H	ID2152_HILIC_pos	530.8375	877.2995	unknown
203	4H	ID196_HILIC_pos	44.9749	163.1463	unknown
204	4H	ID1912_HILIC_pos	254.2377	763.599	unknown
205	4H	ID1906_HILIC_pos	253.9488	762.5947	PC34:0
206	4B/4H	ID1904_HILIC_pos	253.4206	761.5871	unknown
207	4H	ID1889_HILIC_pos	253.2523	758.5674	PC(34:2)
208	4H	ID1858_HILIC_pos	256.0458	736.572	unknown
209	4H	ID1855_HILIC_pos	255.7154	735.5715	unknown
210	4H	ID1852_HILIC_pos	47.5158	734.5681	PC(32:0)
211	4H	ID1850_HILIC_pos	253.782	734.5695	PC(32:0)
212	4B/4H	ID176_HILIC_pos	427.8128	160.1324	Aminovaleric acid betaine (could be 4- or 5-)
213	4H	ID1581_HILIC_pos	44.1712	634.6276	unknown
214	4H	ID1501_RP_pos	583.4205	428.3723	Octadecanoyl-L-carnitine
215	4H	ID1182_HILIC_pos	471.4868	495.1841	unknown
216	4B/4H	ID1058_HILIC_pos	42.9742	444.3705	unknown
Fig4B	4B	ID397_HILIC_pos	357.6501	245.0794	unknown
Fig4B	4B	ID162_HILIC_pos	45.5128	153.1254	unknown
Fig4B	4B	ID978_HILIC_pos	43.2362	428.3824	unknown
Fig4B	4B	ID920_HILIC_pos	60.6639	418.1883	unknown
Fig4B	4B	ID322_RP_neg	516.766	399.1485	unknown
Fig4B	4B	ID2150_HILIC_pos	529.651	876.2944	unknown

758 # STAR Methods

759 **Ethics**
760 The study was carried out in accordance with the Declaration of Helsinki and was approved by
761 the Ethics committee of the Technical University of Munich under the study number 254/17S
762 and included the written informed consent of the parents or legal guardians of the participating
763 infants. The study is registered at the German Clinical Trials Registry (DRKS00012313).

764 **Study participants**
765 Healthy women in their third trimester of pregnancy were recruited in the greater Munich,
766 Germany area and eligibility for participation in the study was assessed. Exclusion criteria were
767 premature birth (gestational age being less than 37 weeks), physical deformities that affect
768 feeding (such as cleft lip and palate) and serious medical conditions that required an intensive
769 care stay exceeding 3 days. Based on current healthcare guidelines in Germany, parents were
770 explicitly encouraged to breastfeed. For participation in the study, parents agreed to use the
771 provided study infant formula in case formula feeding became necessary.

772 **Controlled intervention trial design**
773 The Infantibio-II study was a double-blind, randomized and placebo-controlled interventional
774 trial. Infant fecal samples were collected at age 0.5, 1, 3, 7 and 12 months with an additional,
775 voluntary follow-up sample at age 2 years. Infants were randomized to one of four formula
776 groups. The letters A-D were used for blinding of the different formula groups. Formula group
777 A (placebo) contained no additional supplements. Formula group B contained two bacterial
778 isolates from native fecal samples of infants[10] belonging to the species *Bifidobacterium longum*
779 subsp. *infanti*s and *B. breve*. Lactosan International GmbH & Co. used freeze-dried bacterial
780 powder to supplement infant formula with 10^7 cfu/g of each strain. Formula group C contained
781 a syrup-based galacto-oligosaccharide (GOS) mixture (5g/L, FrieslandCampina). Formula
782 group D contained both *Bifidobacterium* strains and GOS. Parents were free to decide if, when
783 and how much formula was fed to the infants in addition to or after cessation of breastfeeding.
784 The reference group were infants that were fully breastfed for the entirety of the study period
785 with the exception of solid food in addition to breastmilk.

786 **Infant formula**
787 Infant formula was manufactured by Töpfer GmbH (Dietmannsried, Germany) and provided
788 blinded to the study team for distribution to participants. The four formulas could not be
789 distinguished from one another by looks, smell or other characteristics. Unblinding of formula
790 groups took place after study completion. The study formula was a powdered organic cows-
791 milk based infant formula containing all the necessary nutrients based on laws and regulations
792 at the time of manufacturing (2018-2020). Parents received detailed instructions on how to
793 prepare drink-ready formula including a digital thermometer for correct preparation.

794 **Fecal sample collection**
795 Parents collected fecal samples from the diapers of participating infants and recorded the time
796 of sampling. Stool sampling kits were provided including collection tubes with DNA stabilizing
797 solution (Invitek Moleculuar, 1038111300) and empty fecal collection tubes (Süsse
798 Labortechnik, H8555T). Two spoons of fecal matter were added to the tubes and immediately
799 refrigerated until pick-up by study team, latest 24 hours after defecation. Samples were
800 aliquoted and stored at -80°C at the study center at the Technical University Munich in Freising,
801 Germany (ZIEL- Institute for Food & Health). Case report forms detailing birth characteristics,

802 familial health status, environmental factors and the current feeding habits of the infant were
803 completed at enrollment of study and with every stool sample collection. Parental fecal samples
804 (86 from mothers and 66 from fathers) were collected on a voluntary basis upon consent at the
805 infant sample time point 1-month according to previously established protocols.[51]

806 **16S rRNA gene amplicon sequencing and analysis**

807 Metagenomic DNA was isolated from 600 µl fecal matter in DNA stabilizing solution using a
808 previously described DNA-isolation protocol.[51] Negative controls in form of DNA extracted
809 from water and DNA extracted from stool stabilizer (without fecal matter) were included every
810 45 samples. DNA extraction was followed by two-step polymerase chain reaction (PCR)
811 amplification and sequencing on Illumina HiSeq in paired-end mode (2x 250 bp) using the
812 HiSeq Rapid Kit v2 from Illumina.[51]

813 The UPARSE-based[52] platform "Integrated Microbial Next Generation Sequencing"
814 (IMNGS)[53] was adapted as an in-house offline version (NGSToolkit, v6.0.2-beta.5) for
815 processing the sequencing output. Reads were trimmed to the first base. USEARCH 8.0[54] was
816 used for paring of samples with 1 allowed mismatch per barcode. Remaining reads were
817 trimmed (5 nucelotides each) followed by denoising and clustering by 100% identity, creating
818 zero-radius operational taxonomic units (zOTUS) for optimal resolution of microbial strains in
819 16S rRNA sequencing. Chimera sequences were removed using UCHIME.[55] Following best
820 practices, zOTUs with a relative abundance below 0.25% were removed.[56] Taxonomic labels
821 were assigned by SINA 1.6.1 with the SILVA database (release 128).[57] The sequences of a
822 subset of zOTUs of interest were identified using the EzBioCloud database.[58] Maximum-
823 likelihood phylogeny calculations were done with FastTree[59] and visualized with EvolView.[60]
824 Longitudinal changes in microbial abundances were visualized using horizon plots generated
825 with the BiomeHorizon R package (v1.0.0).[61]

826 RHEA was used for microbial profile analysis.[62] Statistical analysis was performed in
827 GraphPad Prism, version 9.4.1 (GraphPad Software, LLC) or in R (2022.02.3+492).
828 Normalization (no random subsampling, no rounding; cutoff was set to 10000 reads for 1st year
829 samples, 20000 reads in case of the fermenter samples and infant samples including the 24-
830 month samples. The different thresholds were chosen in relation to the number of reads of each
831 dataset.) and analysis such as alpha- and beta-diversity as well as taxonomic binning were
832 performed with Rhea. Correction for multiple testing was done with Benjamini-Hochberg
833 procedure. For comparison between more than two groups, a one-way ANOVA was used for
834 normally distributed data (Shapiro Wilk test, alpha = 0.05). Otherwise, we used a Kruskal-
835 Wallis test with Dunn's procedure as post-hoc multiple comparison test. Stars indicate
836 significance level: *$p < 0.05$; **$p < 0.01$; ***$p < 0.001$. The "NBClust (v3.0)" package in R
837 was used for hierarchical clustering of samples. The optimal number of clusters was determined
838 based on the Calinski and Harabasz index[63] and Ward's hierarchical clustering criterion.[64]
839 Differences in microbial composition were calculated using a PERMANOVA test on
840 generalized UniFrac distances, where the length of the bar in the graph provides context for
841 dissimilarities of samples.

842 PICRUSt2 (v2.4.2)[65] was used for functional analysis on all zOTUs identified in infant samples.
843 zOTU sequences were used for predicting Metacyc pathway abundances (Caspi, Billington et
844 al. 2018) without considering super-classes. The estimated Metacyc pathway abundances were
845 used as a basis for linear discriminant analysis (LDA) effect size (LEfSe) calculations (alpha:
846 0.01) comparing formula group A to the other feed groups.[66]

847 The bacterial transmissibility ratio (%) between mother and infant was determined based on the
848 number of shared zOTUs present in the mother and the child divided by the total number of
849 zOTUs present in the mother. A non-parametric Kruskal-Wallis test followed by a post-hoc
850 Dunn test was used to assess the significance between the groups.

851 **Diurnal and circadian analysis of infant microbiota and *in vitro* samples**
852 To identify diurnal rhythms, a cosine-wave equation with a fixed 24-h period:
853 y = baseline + (amplitude*cos(2*π*((x-[phase shift)/24))) was fitted on alpha-diversity, taxa
854 level and relative abundance of individual zOTUs. Significance was determined with an F-Test
855 and goodness of fit was corrected for multiple testing. Significant rhythmicity was assumed to
856 occur when $p \leq 0.05$. An adjusted version of the "CompareRhythms" script[67] created for
857 circadian rhythm comparison between groups, which performs JTK_cycle[68] followed by
858 DODR.[69] Heatmaps were created using the heatmap script in R. The amplitude shown in the
859 Manhattan plot is based on JTK_cycle and the phase is calculated using cosine-wave regression.
860 Circadian cosine-fitting for *in vitro* sample was performed using an in-house code by Isaiah
861 Ting based on.[70]

862 **Shallow metagenomics sequencing**
863 To further enhance the identification and the understanding of the role of individual bacterial
864 strains, shallow shotgun metagenomic sequencing was performed using isolated gDNA on a
865 NovaSeq machine (1G raw data with paired-end 150 bp) on a subset of paired infant samples
866 at time points month 3 and month 7. The resulting metagenomic data was demultiplexed and
867 from the raw sequencing reads adapters were trimmed using "Trim Galore" (developed by F.
868 Krueger, The Babraham Institute: https://github.com/FelixKrueger/TrimGalore, v.0.6.7).
869 Quality control of sequencing reads (removal of low-quality reads and contaminants) was done
870 using the pipeline "Knead data" (https://github.com/biobakery/kneaddata, v.0.7.7-alpha).
871 Species-level taxonomic annotation was done using MetaPhlan 3.0.13 and HUMAnN 3.0.[71]
872 Gene families that were detected via HUMAnN 3.0 were mapped to the KEGG pathway
873 orthologs.[72] Centered log ratio scaling was applied.

874 **Untargeted metabolomics**
875 Sample preparation: 100 mg native infant fecal matter was added to a 15 ml tube (CKMix 50,
876 Bertin Technologies) containing ceramic beads (mixture of 2.8 mm and 5.0 mm beads). Then,
877 5 ml of methanol-based dehydrocholic acid extraction solvent (c = 1.3 µmol/L) was added and
878 the sample was homogenized using a bead beater system (Precellys Evolution, Bertin
879 Technologies) with a cooling adapter containing liquid nitrogen (Bertin Technologies). The
880 bead beating procedure was performed three times per sample for 20 seconds at 10 000 rpm
881 with a 15 second break between each round of bead beating. The sample was then centrifuged
882 at 8 000 rpm for 10 minutes at 10°C. 500 ml of clear supernatant was transferred to a LC-
883 MS/MS vial for untargeted metabolomics analysis. Multiple smaller volumes of samples were
884 pooled to prepare a QC-sample.

885 Untargeted mass spectrometric measurement**:** analysis was performed using a Nexera UHPLC
886 system (Shimadzu, Duisburg, Germany) coupled to a Q-TOF mass spectrometer (TripleTOF
887 6600 AB Sciex, Darmstadt, Germany). Separation of the stool samples was performed either
888 using a UPLC BEH Amide 2.1 × 100 mm, 1.7 µm analytic column (Waters, Eschborn,
889 Germany) with a 400 µL/min flow rate or with a Kinetex XB18 2.1 x 100 mm, 1.7 µm
890 (Phenomenex, Aschaffenburg, Germany) with a 300 µL/min flow rate. For the HILIC-
891 separation the settings were as follows. The mobile phase was 5 mM ammonium acetate in

892 water (eluent A) and 5 mM ammonium acetate in acetonitrile/water (95/5, v/v) (eluent B). The
893 gradient profile was 100% B from 0 to 1.5 min, 60% B at 8 min and 20% B at 10 min to 11.5 min
894 and 100% B at 12 to 15 min. For the reversed-phase separation eluent A was 0.1% formic acid
895 and eluent B was 0.1% formic acid in acetonitrile. The gradient profile started with 0.2% B
896 which was held for 0.5 min. Afterwards the concentration of eluent B was increased to 100%
897 until 10 min which was held for 3.25 min. Afterward the column was equilibrated at starting
898 conditions. A volume of 5 µL per sample was injected. The autosampler was cooled to 10 °C
899 and the column oven heated to 40 °C. Every tenth run a quality control (QC) sample which was
900 pooled from all samples was injected. The samples were measured in a randomized order and
901 in the Information Dependent Acquisition (IDA) mode. MS settings in the positive mode were
902 as follows: Gas 1 55, Gas 2 65, Curtain gas 35, Temperature 500 °C, Ion Spray Voltage 5500,
903 declustering potential 80. The mass range of the TOF MS and MS/MS scans were 50–2000 m/z
904 and the collision energy was ramped from 15–55 V. MS settings in the negative mode were as
905 follows: Gas 1 55, Gas 2 65, Cur 35, Temperature 500 °C, Ion Spray Voltage –4500,
906 declustering potential –80. The mass range of the TOF MS and MS/MS scans were 50–
907 2000 m/z and the collision energy was ramped from –15–55 V.

908 Data processing: The "msconvert" from ProteoWizard[73] was used to convert raw files to
909 mzXML (de-noised by centroid peaks). The bioconductor/R package xcms[74] was used for data
910 processing and feature identification. More specifically, the matched filter algorithm was used
911 to identify peaks (full width at half maximum set to 7.5 seconds). Then the peaks were grouped
912 into features using the "peak density" method.[74] The area under the peak was integrated to
913 represent the abundance of features. The retention time was adjusted based on the peak groups
914 present in most samples. To annotate features with names of metabolites, the exact mass and
915 MS2 fragmentation pattern of the measured features were compared to the records in HMBD[75]
916 and the public MS/MS spectra in MSDIAL,[76] referred to as MS1 and MS2 annotation,
917 respectively. Missing values were imputed with half of the limit of detection method, i.e., for
918 every feature, the missing values were replaced with half of the minimal measured value of that
919 feature in all measurements. To confirm a MS2 spectra is well annotated, we manually reviewed
920 our MS2 fragmentation pattern and compared it with records in the public database, using
921 SIRIUS[77] or previously measured reference standards to evaluate the correctness of the
922 annotation. The mass spectrometric data is made publically available using the massive
923 repository (https://massive.ucsd.edu) under the accession number MassIVE MSV000093140
924 for the feces data and MassIVE MSV000093802 for the breastmilk and formula data.

925 **Metabolite analysis**

926 To obtain information about potential associations between metabolites and species (data from
927 shallow metagenomic sequencing) or zOTUs (data from 16S sequencing), network analysis was
928 performed. For this, a correlation matrix was calculated. A spearman correlation was calculated
929 and only features with a significant correlation and an absolute correlation value above 0.5 were
930 selected. For plotting of the network, the R qgraph version 1.9 was used. Therefore payout
931 spring was used, with a minimum absolut edge weight of 0.5.

932 Data from positive, negative and reverse phase were merged, i.e. some of the metabolites might
933 appear more than once (due to being detected in different phases). To reduce the number of
934 metabolites according to the post prevalent metabolites, the input tables were ordered by
935 decreasing sum over all individuals. Afterwards a spearman correlation was calculated and used
936 for further analysis. For 4F a subset of significantly different species was selected. Based on
937 this subset a correlation matrix was calculated. In the heatmaps, only significant and high

938 correlated (absolute correlation coefficient above 0.5) species - metabolites correlations are
939 shown.

940 ***Ex vivo* Infant Colonic Continuous Fermentation**

941 Infant Stool Samples Selection, Preparation, and Inoculation**:** Fecal samples of two 3-month
942 old infants, one exclusively breast-fed and one exclusively fed with formula A, were selected
943 to be representative of their feeding group based on Principal Component Analysis (PCA) and
944 *Bifidobacterium* abundance. Fecal slurries were prepared under anaerobic conditions by
945 diluting each sample (previously thawed on ice and weighted: BF = 1.03 g, A = 1.98 g) in
946 reduced PBS (3% L-Cys HCl). Each slurry was filtered (70 µm cell strainer) and an equal
947 amount was loaded in two syringes to be injected in duplicate chemostat vessels (BF =
948 2x6.5mL, A = 2x8mL). The whole procedure was finished ~1.5 hours after the samples were
949 thawed.

950 Preparation of the Culture Medium: A modified culture medium was prepared to mimic the
951 physiological conditions of the infant colon. The media composition was based on the
952 composition and calculations described in literature[78] adapted to the composition of the infant
953 formula A. A fat content of 10% was chosen for this experiment,[79] and a full nutrient ratio of
954 carbohydrate:nitrogen:fats after digestion with 13 g/L of carbohydrates was adjusted to
955 44:46:10 (corresponding to 11.88 g/L of fat). Therefore, the total concentration of undigested
956 compounds in the medium were 2.96 g/L of total fat and 13.72 g/L of undigested N-compounds.
957 The full composition of the culture medium, in g/L, was as follows (all the medium components
958 were provided by Sigma-Aldrich, unless specified otherwise): *base media* (NaCl: 4.47; KCl:
959 4.43; $MgSO_4$: 1.24; $CaCl_2$: 0.1; $NaHCO_3$: 1.5; KH_2PO_4: 0.5; $FeSO_4$: 0.005; Bile salts: 0.05;
960 Tryptone: 0.5; Peptone: 0.5; Yeast Extract: 2.5; Tween 80: 1; L-carnitine: 0.0015); *mucin media*
961 (porcine gastric mucin type II: 4); and *milk media* (whey protein hydrolysate (Myprotein, UK):
962 11.21; casein: 0.47; pre infant formula A: 11.88). Each solution was sterilized by autoclaving
963 at 121ºC for 15 min (110ºC for *milk media* after adjusting pH to 8.0[80] and then mixed
964 thoroughly. Two solutions were added after sterile filtration (0.2 µm): the first containing 0.8
965 g/L of L-cysteine, 5.86 g/L of lactose, and 0.004 g/L of inositol and the second was a vitamin
966 solution as prepared by[81] which also included hemin (0.01 g/L).

967 *Ex vivo* gut chemostat: The two infant fecal samples were cultured in duplicate chemostats
968 (Bioreactor Model Multifors 2, Infors HT, Switzerland) according to the illustrated
969 experimental scheme (**Fig. 5G**). In the first stage of the *ex vivo* gut chemostat model, a batch
970 culture (total 48 h) was employed to allow for sample adaptation after inoculation. After 24 h
971 without adjustment of pH or flow of fresh culture medium, the culture volume in the bioreactors
972 were doubled and maintained at 800 mL until the end of the batch culture. In the second stage
973 of the gut chemostat, a continuous culture was established for 7 days applying a retention time
974 of 12.5 h.[78] Samples were taken once each day at the same time (1.5 mL for DNA extraction
975 and 16S rRNA Sequencing). Finally, the third stage were 48 hours of rhythmicity sampling
976 during which samples were taken every 4 h. The following conditions were applied during the
977 9 days of continuous culturing: 400 mL of volume in the bioreactors, feed rate of 32
978 ml/h/chemostat, pH was set to 6.5 and then maintained (pH electrodes, Hamilton, Germany).
979 Temperature was kept at 37ºC, anaerobic conditions were controlled by supplying a continuous
980 flow of N_2 and redox values were measured (Redox electrodes, 1 per chemostat, Hamilton,
981 Germany).

982 **References STAR Methods**

983 10. Bazanella, M., Maier, T.V., Clavel, T., Lagkouvardos, I., Lucio, M., Maldonado-Gòmez, M.X.,
984 Autran, C., Walter, J., Bode, L., and Schmitt-Kopplin, P. (2017). Randomized controlled trial
985 on the impact of early-life intervention with bifidobacteria on the healthy infant fecal microbiota
986 and metabolome. The American journal of clinical nutrition *106*, 1274-1286.
987 51. Reitmeier, S., Kiessling, S., Neuhaus, K., and Haller, D. (2020). Comparing circadian
988 rhythmicity in the human gut microbiome. STAR protocols *1*, 100148.
989 52. Edgar, R.C. (2013). UPARSE: highly accurate OTU sequences from microbial amplicon reads.
990 Nature methods *10*, 996-998.
991 53. Lagkouvardos, I., Joseph, D., Kapfhammer, M., Giritli, S., Horn, M., Haller, D., and Clavel, T.
992 (2016). IMNGS: A comprehensive open resource of processed 16S rRNA microbial profiles for
993 ecology and diversity studies. Scientific reports *6*, 33721.
994 54. Edgar, R.C. (2010). Search and clustering orders of magnitude faster than BLAST.
995 Bioinformatics *26*, 2460-2461. 10.1093/bioinformatics/btq461.
996 55. Edgar, R.C., Haas, B.J., Clemente, J.C., Quince, C., and Knight, R. (2011). UCHIME improves
997 sensitivity and speed of chimera detection. Bioinformatics *27*, 2194-2200.
998 56. Reitmeier, S., Hitch, T.C., Fikas, N., Hausmann, B., Ramer-Tait, A.E., Neuhaus, K., Berry, D.,
999 Haller, D., Lagkouvardos, I., and Clavel, T. (2020). Handling of spurious sequences affects the
1000 outcome of high-throughput 16S rRNA gene amplicon profiling.
1001 57. Pruesse, E., Peplies, J., and Glöckner, F.O. (2012). SINA: accurate high-throughput multiple
1002 sequence alignment of ribosomal RNA genes. Bioinformatics *28*, 1823-1829.
1003 58. Yoon, S.-H., Ha, S.-M., Kwon, S., Lim, J., Kim, Y., Seo, H., and Chun, J. (2017). Introducing
1004 EzBioCloud: a taxonomically united database of 16S rRNA gene sequences and whole-genome
1005 assemblies. International journal of systematic and evolutionary microbiology *67*, 1613.
1006 59. Price, M.N., Dehal, P.S., and Arkin, A.P. (2010). FastTree 2–approximately maximum-
1007 likelihood trees for large alignments. PloS one *5*, e9490.
1008 60. Subramanian, B., Gao, S., Lercher, M.J., Hu, S., and Chen, W.-H. (2019). Evolview v3: a
1009 webserver for visualization, annotation, and management of phylogenetic trees. Nucleic acids
1010 research *47*, W270-W275.
1011 61. Fink, I., Abdill, R.J., Blekhman, R., and Grieneisen, L. (2022). BiomeHorizon: visualizing
1012 microbiome time series data in R. Msystems *7*, e01380-01321.
1013 62. Lagkouvardos, I., Fischer, S., Kumar, N., and Clavel, T. (2017). Rhea: a transparent and
1014 modular R pipeline for microbial profiling based on 16S rRNA gene amplicons. PeerJ *5*, e2836.
1015 63. Caliński, T., and Harabasz, J. (1974). A dendrite method for cluster analysis. Communications
1016 in Statistics-theory and Methods *3*, 1-27.
1017 64. Murtagh, F., and Legendre, P. (2014). Ward's hierarchical agglomerative clustering method:
1018 which algorithms implement Ward's criterion? Journal of classification *31*, 274-295.
1019 65. Douglas, G.M., Maffei, V.J., Zaneveld, J.R., Yurgel, S.N., Brown, J.R., Taylor, C.M.,
1020 Huttenhower, C., and Langille, M.G. (2020). PICRUSt2 for prediction of metagenome
1021 functions. Nature biotechnology *38*, 685-688.
1022 66. Segata, N., Izard, J., Waldron, L., Gevers, D., Miropolsky, L., Garrett, W.S., and Huttenhower,
1023 C. (2011). Metagenomic biomarker discovery and explanation. Genome biology *12*, 1-18.
1024 67. Pelikan, A., Herzel, H., Kramer, A., and Ananthasubramaniam, B. (2022). Venn diagram
1025 analysis overestimates the extent of circadian rhythm reprogramming. The FEBS journal *289*,
1026 6605-6621.
1027 68. Hughes, M.E., Hogenesch, J.B., and Kornacker, K. (2010). JTK_CYCLE: an efficient
1028 nonparametric algorithm for detecting rhythmic components in genome-scale data sets. Journal
1029 of biological rhythms *25*, 372-380.
1030 69. Thaben, P.F., and Westermark, P.O. (2016). Differential rhythmicity: detecting altered
1031 rhythmicity in biological data. Bioinformatics *32*, 2800-2808.
1032 70. van der Veen, D.R., and Gerkema, M.P. (2017). Unmasking ultradian rhythms in gene
1033 expression. FASEB J *31*, 743-750. 10.1096/fj.201600872R.
1034 71. Beghini, F., McIver, L.J., Blanco-Míguez, A., Dubois, L., Asnicar, F., Maharjan, S., Mailyan,
1035 A., Manghi, P., Scholz, M., and Thomas, A.M. (2021). Integrating taxonomic, functional, and
1036 strain-level profiling of diverse microbial communities with bioBakery 3. elife *10*, e65088.

1037 72. Kanehisa, M., and Goto, S. (2000). KEGG: kyoto encyclopedia of genes and genomes. Nucleic
1038 acids research *28*, 27-30.
1039 73. Kessner, D., Chambers, M., Burke, R., Agus, D., and Mallick, P. (2008). ProteoWizard: open
1040 source software for rapid proteomics tools development. Bioinformatics *24*, 2534-2536.
1041 74. Smith, C.A., Want, E.J., O'Maille, G., Abagyan, R., and Siuzdak, G. (2006). XCMS: processing
1042 mass spectrometry data for metabolite profiling using nonlinear peak alignment, matching, and
1043 identification. Analytical chemistry *78*, 779-787.
1044 75. Wishart, D.S., Feunang, Y.D., Marcu, A., Guo, A.C., Liang, K., Vázquez-Fresno, R., Sajed, T.,
1045 Johnson, D., Li, C., and Karu, N. (2018). HMDB 4.0: the human metabolome database for 2018.
1046 Nucleic acids research *46*, D608-D617.
1047 76. Tsugawa, H., Cajka, T., Kind, T., Ma, Y., Higgins, B., Ikeda, K., Kanazawa, M.,
1048 VanderGheynst, J., Fiehn, O., and Arita, M. (2015). MS-DIAL: data-independent MS/MS
1049 deconvolution for comprehensive metabolome analysis. Nature methods *12*, 523-526.
1050 77. Dührkop, K., Fleischauer, M., Ludwig, M., Aksenov, A.A., Melnik, A.V., Meusel, M.,
1051 Dorrestein, P.C., Rousu, J., and Böcker, S. (2019). SIRIUS 4: a rapid tool for turning tandem
1052 mass spectra into metabolite structure information. Nature methods *16*, 299-302.
1053 78. Cinquin, C., Le Blay, G., Fliss, I., and Lacroix, C. (2004). Immobilization of infant fecal
1054 microbiota and utilization in an in vitro colonic fermentation model. Microbial ecology *48*, 128-
1055 138.
1056 79. Wieczorek-Filipiak, M., Drzymala-Czyz, S., Szczepanik, M., Szydlowski, J., Walkowiak, D.,
1057 Nowak, J.K., Moczko, J.A., and Walkowiak, J. (2019). Fecal fat concentration and excretion in
1058 the first 2 years of life: a cross-sectional study. Journal of Pediatric Gastroenterology and
1059 Nutrition *68*, 285-289.
1060 80. Pelegrine, D.H.G., and Gomes, M.T.M.S. (2012). Analysis of Whey Proteins Solubility at High
1061 Temperatures. International Journal of Food Engineering *8*. doi:10.1515/1556-3758.1265.
1062 81. Gibson, G.R., and Wang, X. (1994). Enrichment of bifidobacteria from human gut contents by
1063 oligofructose using continuous culture. FEMS microbiology letters *118*, 121-127.

1064